Sex Dependent Effects of Amyloid Precursor-Like Protein 2 in The SOD1-G37R Transgenic Mouse Model of MND.

Phan Hong Truong (phan.truong@florey.edu.au)
Florey Institute of Neuroscience and Mental Health - Austin Campus https://orcid.org/0000-0002-9964-0678

Peter J. Crouch
The University of Melbourne

James B.W. Hilton
The University of Melbourne

Catriona A. McLean
Alfred Hospital

Roberto Cappai
The University of Melbourne

Giuseppe D. Ciccotosto
The University of Melbourne

Research article

Keywords: Amyloid Precursor Protein, Amyloid Precursor-Like Protein, knockout, motor neuron disease, SOD1-G37R, sex differences, amyotrophic lateral sclerosis

Posted Date: March 30th, 2021

DOI: https://doi.org/10.21203/rs.3.rs-343057/v1

Abstract

Introduction:

Motor neurone disease (MND) is a neurodegenerative disorder characterised by progressive destruction of motor neurons, muscle paralysis and death. The amyloid precursor protein (APP) is highly expressed in the central nervous system and has been shown to modulate disease outcomes in MND. APP is part of a gene family that includes the amyloid precursor-like protein 1 (APLP1) and 2 (APLP2) genes.

Methods

In the present study, we investigated the role of APLP2 in MND through the examination of human spinal cord tissue and by crossing APLP2 knockout mice with the superoxide dismutase 1 (SOD1-G37R) transgenic mouse model of MND.

Results

We found the expression of APLP2 is elevated in the spinal cord from human cases of MND and that this feature of the human disease is reproduced in SOD1-G37R mice at the end-stage of their MND-like phenotype progression. APLP2 deletion in SOD1-G37R mice significantly delayed disease progression and increased the survival of female SOD1-G37R mice. Molecular and biochemical analysis showed female SOD1-G37R:APLP2-/- mice displayed improved innervation of the neuromuscular junction, ameliorated atrophy of muscle fibres with increased APP protein expression levels in the gastrocnemius muscle.

Conclusion

These results indicate a sex-dependent role for APLP2 in mutant SOD1-mediated MND and further support the APP-family as a potential target for further investigation into the cause and regulation of MND.

Background

Motor neurone disease (MND) is a fatal human neurodegenerative disorder, and the most common form of MND is amyotrophic lateral sclerosis (ALS) (1) MND is characterised by the progressive destruction of motor neurons in the central nervous system (CNS) which causes muscle weakness, muscle atrophy, paralysis and ultimately death (2). Despite progress in deciphering the molecular mechanisms of this disease, the cause and modulation of MND pathogenesis remains unclear. While the sporadic causes triggering this disease account for the majority of patients diagnosed with MND, 5–10% of cases are inherited as familial MND (3).

MND patients display clinical heterogeneity with differences in the anatomical site of disease onset, symptom severity and rate of disease progression (4, 5) while age, sex, and various molecular targets are also contributing factors (6, 7). This disease is predominantly presented in adulthood at around 55–70 years of age while a relatively small percent (~ 5%) of patients diagnosed with MND are around 20–30 years of age and in extremely rare cases, patients have been diagnosed before the age of 20 (8, 9). Sex affects the incidence, clinical presentation and severity of the MND with men affected at 1.5-fold higher rate compared to women (5, 10). However, this sex difference diminishes at post-menopausal ages (11) suggesting a protective role by estrogens in MND pathophysiology (7). Sexual dimorphism in clinical phenotypes has been described in several studies, and they all consistently show a higher incidence of limb onset in men (12) while bulbar onset is more frequent in women (13, 14). In rodent animal models, sex differences have been reported to occur in transgenic SOD1-G93A mice (15, 16) with the females displaying longer lifespans due to delayed symptom onset (17). However, disparity in the literature exists, with some reporting that the onset of motor symptoms was detected earlier in male than in female SOD1-G93A mice (18). The occurrence of sex differences in MND subjects makes sex comparison an important variable to be investigated in basic and preclinical research.

Several molecular factors have been identified that can modulate MND disease outcomes. One of these includes *Bax*, an important gene involved in the activation of the mitochondrial apoptosis pathway, where its deletion in the SOD1-G93A mice caused a delayed onset of disease symptoms and moderately increased its lifespan but failed to alter disease duration (19). Similarly, the deletion of BH3-only protein, a pro-apoptotic protein important in regulating endoplasmic reticulum stress, in SOD1-G93A mice, improved motor neuron survival, delayed symptom onset and motor dysfunction, but failed to improve the lifespan in these mice too (20). In contrast, the deletion of the PrP gene in SOD1-G93A mice significantly accelerated disease progression resulting in reduced lifespan (21). Among these molecular modifiers, the amyloid precursor protein (APP), best known for its involvement in Alzheimer's disease pathogenesis, has been shown to modulate disease progression in SOD1-G93A mice (22). Apart from being a genetic modifier, APP expression is associated with many physiological and pathological roles in the CNS and peripheral nervous systems (PNS). For example, following traumatic brain injury (TBI), APP protein expression levels are increased at the site of impact as part of a neuroprotective response (23). APP expression is also upregulated in motor neurons undergoing programmed cell death as well as in ageing and injured neurons (24, 25). Similarly, APP protein levels are upregulated in postmortem spinal cord and muscle tissues in MND patients (26, 27) and in the rodent model for MND (SOD1-G93A mouse) at symptomatic age (26–28). Moreover, a pilot study of MND patients revealed elevated levels of soluble APP cleavage products with a shift towards the non-amyloidogenic pathway of APP processing (29). Regulating APP expression may have beneficial effects in MND since genetic deletion of APP (APP-/-) in the SOD1-G93A mice significantly slowed disease progression and promoted motor neuron survival, while the neuromuscular junction (NMJ) innervations in SOD1-G37R:APP-/- mice showed reduced denervation and improved muscle contractility (22). Taken together, these observations indicate the potential involvement of APP in modulating disease progression in MND.

APP is part of a gene family that includes the amyloid precursor-like protein 1 (APLP1) and amyloid precursor-like protein 2 (APLP2) genes. Like APP, APLP2 also possess several important physiological roles that have been characterised in both the CNS and PNS. These include synaptogenesis (30), neurite outgrowth (31), axonal myelination (32), cellular adhesion and signaling (33), neuronal differentiation (34, 35), glucose and insulin homeostasis (36), brain metal homeostasis (37, 38), refractive development (39) and retinal development (40, 41) just to name a few. Therefore, to better understand if modulation of MND extends to other members of the APP-gene family, we investigated the role of APLP2 in the SOD1-G37R transgenic mouse model. To do this, we examined the protein expression profile of both APLP2 and APP in human spinal cord samples from MND subjects and during disease progression in the SOD1-G37R mouse model. We then crossed APLP2 knockout (APLP-/-) mouse with the SOD1-G37R mouse to generate SOD1-G37R mice expressing either two, one or no APLP2 alleles: SOD1-G37R:APLP2+/+, SOD1-G37R:APLP2+/- and SOD1-G37R:APLP2-/- respectively to determine if APLP2 expression affected disease progression by measuring motor function and motor neuron and muscle pathology. We also investigated this in both female and male lines to establish if any effects occurred in a sex-dependent manner.

Materials And Methods

Human spinal cord tissue processing

Frozen sections of lumbar spinal cord were obtained from the Victorian Brain Bank (Australia) and the Multiple Sclerosis (MS) Society Tissue Bank (UK). Tissue samples were stored at -80°C until processed for analysis. Procedures involving handling of post-mortem human tissue were approved by a University of Melbourne Human Ethics Committee (Project ID 1238124). Briefly, human spinal cord tissue samples were homogenised in a tris(hydroxymethyl)-aminomethane-buffered saline (TBS)-based homogenisation buffer and the TBS-insoluble material was collected by centrifugation (21,000 g, 4°C, 15 min). This TBS-insoluble material was then resuspended in TBS-based homogenisation buffer supplemented with 1% (v/v) triton X-100 detergent and the samples centrifuged (18,000 g, 4°C, 5 min) to produce Triton X-100 soluble protein extracts which were assessed for protein content using the Pierce BCA Protein Assay kit, and the protein concentrations across the samples were normalised to a consistent protein concentration by diluting with the Triton X-100 supplemented homogenisation buffer. 10 µg protein samples was separated by gel electrophoresis was performed as previously described (42).

Mice breeding

All mouse experiments in this study complied with the National Health and Medical Research Council code for the care and use of animals for scientific purposes and were approved by the University of Melbourne Animal Ethics Committee (Project Number: 1413304). Mice were housed on a reverse 12/12-hour light/dark cycle with access to feed and water ad libitum. The experimenter was blinded to age and genotype until completion of the behavioural testing. The SOD1-G37R, line 42, stock # 008342 (43), were sourced from The Jackson Laboratory (Bar Harbor, USA), are on a C57BL/6J background and are

hemizygous for the SOD1-G37R transgene. The SOD1-G37R mouse colony was maintained by breeding the hemizygous SOD1-G37R mouse with a non-transgenic C57BL/6J (wild-type, WT) and identifying the hemizygous SOD1-G37R mouse by PCR genotyping. For the SOD1-G37R:APLP2-/- mouse line, the F1 breeding strategy involved mating the SOD1-G37R mouse with a APLP2-/- mouse to generate the WT:APLP2+/- and SOD1-G37R:APLP2+/- progeny at a ratio of 1:1. The F2 breeding strategy involved mating WT:APLP2+/- and SOD1-G37R:APLP2+/- mouse to generate six possible genotypes of equal weighting- 1) SOD1-G37R:APLP2+/+, 2) SOD1-G37R:APLP2+/-, 3) SOD1-G37R:APLP2-/-, 4) WT:APLP2+/+, 5) WT:APLP2+/-, 6) WT:APLP2-/- at 1:6 ratios.

Mice monitoring and end-stage disease

Mouse body weights were recorded weekly and from three weeks of age (at weaning age), the health monitoring frequency was increased to three times per week and then to daily after 25 weeks of age as the MND symptoms became more progressive and severe. Mice were killed when they reached pre-symptomatic (12 weeks), symptomatic (22 weeks) and End-stage (~28 weeks) and similar numbers of control WT mice at similar ages were killed at the same timepoints for direct comparison. End-stage is defined when the mouse met displayed one or more of the following criteria points- no longer able to perform the rotarod task, unable to right itself within 15 sec of being placed on either side, when paralysis was observed in at least one hindlimb or if they lost 15 % of their maximum recorded weight. The same number of WT:APLP2+/+ and WT:APLP2-/- were killed at the same time for age matching. Mice were killed by an intraperitoneal injection of a cocktail of xylazine (16 mg/kg body weight) and ketamine (120 mg/kg body weight) and followed by opening of the pneumothorax and transcardial perfusion with PBS solution.

Neurological scoring in mouse

For each mouse, a neurological score was calculated for both hindlimbs. The neurological scores were assigned using an amended scaling system of the neurological scoring system developed at the ALS Therapy Development Institue (44). Briefly, a score of 0.5 to 1.0 was assigned when the onset motor symptoms, as defined by the mouse displaying tremoring of hind legs and partial collapse of the leg extensions from the lateral midline when suspended by its tail, a score of 1.5-2.0 was assigned when the mouse displayed a complete or partial collapse of hindlimbs, signs of hindlimb muscle atrophy or forelimb tremoring, a sign of toes curling during the tail suspension test or if they curled under at least twice during a 30 centimetre walk or if any part of a foot was dragging along the cage bottom/table), a score of 2.5-3.0 assigned when the mouse developed a very wobbly gait, prominent signs of muscle atrophy in the hindlimb, rigid paralysis or minimal joint movement, foot not being used for generating forward motion or unsteady when walking, and a score 3.5-4.0 assigned when they displayed rigid paralysis and no forward motion, paralysis in one or more limbs, or the mouse cannot right itself within 15 seconds after being placed on either side.

Mouse Rotarod

Locomotor function was assessed using the rotarod instrument (IITC Life Science, Woodland Hills, CA, USA) set to 4 rpm and increasing to 40 rpm over 180 seconds. Prior to testing day, mice were habituated to the instrument for two consecutive days and allowed to explore the apparatus set at a constant speed of 10 rpm for 300 seconds. Following habituation, mice were trained on the rotarod for three consecutive days with the rotation speed initially set to 4 rpm and increasing to 40 rpm over 180 seconds. Mice that were still on the rotarod after 180 seconds were recorded as having no detectable locomotor deficit. Mice that could not continue on the rotarod for the 180 seconds would fall safely on to a padded base. The fall latency was recorded by the experimenter and is defined as the physical fall off the rotarod or if their hindlimbs slip off and they use their front paws remain grasping to the rotarod. Rotarod performances were performed and recorded two days per week, with three trials on each day of testing and intervals of 10 min of rest provided between each test trial. The mice were tested from 8 weeks of age up until the disease End-stage and matching time points in control mice.

Mouse DigiGait

Analysis of the mice's gait was conducted using the DigiGait instrument and analysis performed using the supplied software analysis (Mouse Specifics, Inc, USA). Prior to testing the mice on this instrument, they undergo a pre-training period for 3 days to acclimatize to the instrument and a range of treadmill speeds were tested to determine the maximum speed the mice could tolerate safely. After the training period, DigiGait test recordings were taken for each mouse weekly from 7 weeks of age. Mice were placed on the DigiGait treadmill and setting the belt speed at either 10, 15, 20 cm/s and a 15 second recording taken.

Mouse Tissue collection

Mice were killed and tissues were collected when SOD1-G37R mice reached pre-symptomatic (12 weeks), symptomatic (22 weeks) and end-stage (~28 weeks) and a similar number of control WT mice of similar ages were killed at the same timepoints for direct comparison. For biochemical analysis, the brain, spinal cord, and hindlimb skeletal muscle organs were dissected free, immediately snap frozen in liquid nitrogen and then transferred to clean tubes for storage at -80C until processing. For histological analysis, the spinal cord tissue was carefully removed from the spinal cord canal and the lumbar region identified and dissected free and postfixed in freshly prepared 4% paraformaldehyde in PBS solution overnight then cryo-protected by incubation in a 30% sucrose solution (v/v in PBS) for at least 24 hours. The harvested lumber spinal cord or hindlimb skeletal muscle (which were laid flat on the end of a syringe) were embedded in Optimal Cutting Temperature compound (Tissue-Tek; Sakura FineTek) and snap frozen in a bath of isopentane pre-chilled in liquid nitrogen and then wrapped in plastic and stored at -80C until cutting for histochemistry.

Mouse tissue processing for biochemical analysis

Brain and spinal cord tissue samples were weighed and lysed at 1:5 w/v in brain lysis buffer (50 mM Tris-HCl, 150 mM NaCl, 0.1% TritonX-100, pH 7.5) by passaging the tissue several times through a series of

18G and 22G needles followed by a homogenization step using a chilled handheld homogenizer that was kept on ice during the procedure. Harvested muscle samples were weighed, minced into very small pieces using a clean sterile scalpel blade while on a petri dish resting on ice, then transferred to a centrifuge tube and muscle lysis buffer added to 1:5 w/v (50 mM Tris-HCl, 150 mM NaCl, 0.1% TritonX-100, 0.1% SDS, 10 mM EDTA, 1 mM dithiothreitol). The tubes were placed in a chilled sonicating water bath and sonicated with three 30 second bursts. To complete homogenization, all homogenate samples were incubated on ice for 20 min then centrifuged at 15,870 g for 30 min at 4°C. The supernatant was transferred to a new tube and the protein concentration quantified using the bicinchoninic acid assay (Pierce, Rockford, IL, USA). Lysis buffer was added to the samples to normalize protein concentration across the samples to 2 mg/ml before gel electrophoresis. Proteins were resolved by SDS-PAGE electrophoresis under reducing and denaturing conditions by pre-mixing equivalent amounts of protein samples with 2X Tris-glycine SDS sample loading buffer (0.16M Tris, 4% SDS, 20% glycerol, 0.04% bromophenol blue). Samples were heated at 95°C for 5 min, allowed to cool for 5 min followed by a quick centrifugation step then loaded into 4-12% NuPAGE Bis-Tris pre-cast gel and the gels were run according to manufacturer's instructions (Invitrogen, Australia). Resolved gels were transferred onto nitrocellulose membranes (BioRad, Australia) using the wet tank blotting system (BioRad, Australia).

Western blot analysis

Briefly, the membranes were incubated in blocking buffer (5% skim milk in PBST (0.05% Tween-20 in PBS) for one hour at room temperature and then probed using an anti-APP antibody 22C11 (APP 66-81) produced in house(45) and an anti-APLP2 95/11 (is a rabbit polyclonal antiserum raised against recombinant APLP2(28-693) protein (46) and expressed in Pichia pastoris (as previously described) (47). GAPDH was detected using Cell Signaling Technology antibody #2118, with HRP-linked anti-rabbit IgG (Cell Signaling Technology, 7074). Blots were incubated in primary antibody diluted in PBST overnight at 4°C, The next day, the membranes were washed in PBST buffer, incubated with a secondary antibody conjugated to horseradish peroxidase for two hours at room temperature and washed in TBST. Immunoreactivity was detected by using the enhanced chemiluminescence reagent (ECL-plus, GE Healthcare, UK) and imaged on a ChemiDoc digital imaging system (BioRad, Australia). Protein expression levels were quantitated by densitometry analysis of band intensities using Image J/Fiji software (ver. 1.52e, NIH). The intensity value for each immune-reactive band was normalised to its corresponding housekeeping loading control to account for variability in protein loading across samples.

Immunohistochemistry of mouse spinal cord sections

Serological transverse tissue sections (1:10) of the lumbar spinal cord were cut at 20 µm thickness (serially) using a cryostat machine (Leica) and were collected and adhered to superfrost plus slides (Fisher Scientific). Immunohistochemistry was prepared by briefly washing sections with PBS buffer three times (5 min per wash), permeabilised (0.3% Triton X in block buffer for 20 min) and blocked (10% goat serum in PBS) for 1 hour. Tissue sections were incubated with primary antibodies to GFAP (Merck Millipore, 1:500), IBA1 (Wako, 1:500), APP (22C11, 1:50, produced in-house) diluted in blocking buffer

overnight at 4°C in a humidifier chamber. The next day, antibodies were removed and slides washed with PBS buffer (three times, 10 min each) before incubation in a secondary goat anti-mouse or goat anti-rabbit antibody (conjugated to horseradish peroxidase (HRP)) for 2 hours at room temperature. Tissue sections were PBS washed (three times, 10 min each) then incubated in DAB enhancement solution (ImmPACT DAB peroxidase-HRP substrate, SK-4105, Vector labs, Australia). Tissue sections were rinsed with distilled water three times then dehydrated in a series of ethanol solutions, cleared in xylene solution two times and mounted in Safety mounting medium (Trajan, Grale). Spinal cord sections were imaged using a digital slide scanner (Panoramic SCAN II, 3Dhistech, Hungary) using a Carl Zeiss Plan Apochromat 20×/NA 0.8 objective (Zeiss, Germany) and the acquired images of tissue sections were viewed using Case Viewer software (ver 2.2, 3Dhistech, Hungary).

Nissl staining of Mouse Spinal cord tissue sections and neuron analysis

Nissl stains were performed to assess neurons in the lumbar sections of the spinal cord. 20 µm thick frozen tissue sections were air dried at RT for 1 h on glass slides, washed in PBS then soaked in 1:1 v/v alcohol/chloroform solution overnight, then rehydrated in a series of ethanol solutions (100%, 90% and 70%) and distilled water. Slides were stained with 0.1% cresyl violet solution (0.1g cresyl violet acetate, 100 ml distilled water, 0.3 ml glacial acetic acid) for 1 hour in a 37 ºC oven. The slides were rinsed in distilled water for three seconds and dehydrated in a series of ethanol solutions (70%, 90% and 100%), cleared in xylene solution two times (5 min each) and mounted in Safety mounting medium (Trajan, Grale). The spinal cord sections were imaged using a digital slide scanner Panoramic SCAN II machine using a Carl Zeiss Plan Apochromat 20×/NA 0.8 objective (Zeiss, Germany). The acquired images were viewed using Case Viewer software (ver 2.2, 3Dhistech, Hungary). For each Nissl stained spinal cord section, the left and right ventral horn regions were selected as regions of interest (ROIs). Neurons were analysed using the manual thresholding command, followed by cell segmentation and particle analysis with neurons having a soma diameter of less than 10 µm excluded from further analysis. A total of seven spinal cord sections were analysed for each animal and the distance between each serial section analysed was at least 200 µm apart.

Neuromuscular junction assessment in mouse tissue

Serological longitudinal sections (1:5) of TA muscle cut at 10 µm thick were collected on superfrost plus slides (Fisher Scientific). Muscle sections prepared for immunofluorescence were fixed in 4% PFA for 1 hour and briefly washed with PBS buffer three times (5 min per wash). All tissue sections were incubated with permeabilisation buffer (0.3% TritonX-100, 10% goat serum in PBS) for 60 min, followed by blocking buffer (10% goat serum in PBS) for 60 min and then in primary antibody diluted in blocking buffer (see Table 2.5 for antibody list) in a humidifier chamber overnight while at 4°C. The following day, diluted antibody was removed, sections washed with PBS buffer three times (10 min per wash) then incubated in a fluoro-tagged secondary antibody (goat anti-mouse or goat anti-rabbit) prepared in blocking buffer and containing DAPI (2 µg/mL) for 1 hour at room temperature and in the dark. Neuromuscular junctions (NMJs) were visualised by adding FITC-alpha-bungarotoxin (CFTM 488A, Biotium, Australia) at 1µg/ml

diluted in blocking buffer solution. All tissue sections were washed with PBS (three times, 10 min each) and then covered with antifade mounting medium (Prolong Gold, Invitrogen) and mounted with a glass coverslip. The slides were air dried at room temperature for at least 24 hours in the dark before imaging. The stained tissue sections were visualised through a 20X objective using a Zeiss Axioplan 2 microscope and images taken with a Coolscope snap camera and Zen 2 software (Zeiss, Germany). The same exposure settings were used for all mice genotypes and exported in a TIF format, and the fluorescence intensity levels quantified using Image J/Fiji software (ver. 1.52e, NIH).

The innervation status of each NMJ was assessed by determining the level of co-localisation between the muscle fibre end plate (α-bungarotoxin, green) and axon terminal of motor neuron (synaptophysin, red). Co-localisation levels were measured using Imaris software (ver. 9.1, Bitplane, USA) and greater than 150 NMJs were examined in each animal for analysis. For each NMJ, two separate surfaces were created for each channel to allow the creation of a co-localisation surface containing the overlapped region of the two surfaces. The volume of the three surfaces was used to calculate the percentage of co-localization or NMJ innervation.

ATPase staining for mouse muscle tissue

The muscle fibre types in the gastrocnemius (GA) muscle located in the mouse hindlimb, were analysed by histochemical staining for myosin ATPase activity based on a previously published protocol (48). Briefly, serological transverse sections (1:10) of the GA muscle was cut at 20 µm thickness and adhered to Superfrost plus glass slides (Fisher Scientific) by incubation at room temperature for 1 hour. Slides were washed in PBS then fixed in 4% paraformaldehyde solution (prepared in PBS) for 1 hour and then washed with PBS three times. Two sets of muscle slides were incubated in Myosin ATPase activity buffer with 1 slide set incubated in buffer at pH 4.3 and the second slide incubated in a buffer set at pH 10.2. For Myosin ATPase pH 4.3 treatment, slides were pre-incubated in 0.1M acetate buffer at pH 4.3 for 10 min and for Myosin ATPase pH 10.2, slides were pre-incubated in Baker's Formal Calcium solution for 1 min. Slides from both sets were then briefly washed in distilled water and placed in sodium barbital solution and incubated at 37°C for 30 min. Slides were brought to room temperature and washed in distilled water three times, incubated in fresh 1% $CaCl_2$ for 10 min followed by incubation in 2% $CoCl_2$ for 10 min. Slides were washed thoroughly in distilled water and the colour allowed to develop for 15 seconds in freshly prepared 1% ammonium sulfide solution in a fume cupboard and then slides were washed with distilled water. Slides were dehydrated through the series of 70%, 90% and 100% alcohol solutions, cleared with xylene and finally mounted in safety mounting medium (Trajan, Grale) with a glass coverslip.

Mouse Muscle fibre typing analysis

Stained muscle sections were imaged using a Zeiss Axioscope 2 light microscope through a 10X objective and images were acquired using Axiocam 503 colour camera with Zenpro software 2011 (Zeiss, Germany). Acquired images were exported in TIF format and imported into Image J/Fiji software (ver.

1.52e, NIH) for further analysis. Total fibre numbers and the composition of each fibre type group were counted manually using the cell counter function. For each muscle fibre type, the cross-sectional area of each muscle fibre cell was measured using ROI function. Over 150 muscle cells were measured per animal.

Statistical analysis

All data are expressed as mean ± SEM with p values of 0.05 or less considered as significant. A student's *t-test* was used to compare between two experimental groups. Multiple comparisons were assessed using a one-way analysis of variance with Bonferroni's post-hoc test to compare different genotypes within the same sex groups. A two-way analysis of variances was used when assessing between different genotypes, age and sex, followed by Tukey's post-hoc tests. To determine the time in which mice showed a reduction in their rotarod performance, a split line regression model using GenStat (ver. 6, VSN International, UK) analysis package was used to fit the performance curve for each animal followed by Student's *t-test* using GraphPad Prism software (Ver. 7, San Diego, CA, USA) to compare between 2 sex groups. All other statistical analyses were performed using GraphPad Prism software.

Results

APLP2 and APP protein expression are upregulated in the human MND spinal cord.

We assessed the protein expression levels of APLP2 and APP proteins in post-mortem spinal cord samples from human MND cases and compared them to age matched healthy control samples (Table 1, Figure 1). Our results for the APLP2 protein expression level in the MND patient group were 1.8 fold-higher and significantly different compared to the control group (Figure 1A). Like APLP2, the APP protein expression levels are congruent with those previously reported (26, 27) showing a 2.3-fold and higher expression level of APP in the MND affected spinal cord samples and significantly different to the control group (Figure 1B).

Table 1. Demographic information of spinal cord samples for control and MND cases.

		Mean		S.D.	
Disease group	**Sex (M:F)**	**Age**	**PMI (h)**	**Age**	**PMI (h)**
Control	1.8 : 1	79.4	37.3	13.1	25.5
MND	2.4 : 1	67.1	34.0	9.0	16.4

PMI: post-mortem interval.

APLP2 and APP protein expression are upregulated at End-stage disease in a sex-dependent manner in the SOD1-G37R mouse

We next assessed the endogenous protein expression level of APLP2 and APP by western blot analysis in the SOD1-G37R mouse at different disease progression time points and compared the results to the age-matched WT littermate controls. Tissue lysates were prepared from organs of the SOD1-G37R mouse model that are most affected by MND; the spinal cord, brain stem, cerebellum and hindlimb muscle. These organs were harvested at three well characterized disease time points termed pre-symptomatic (12 weeks), symptomatic (22 weeks) and End-stage (~28 weeks). In the spinal cord, both APLP2 and APP protein expression levels were significantly elevated in the SOD1-G37R mouse at End-stage ($p<0.05$) compared to the age-matched WT control mouse (Figure 2A) and demonstrating the recapitulation of this human disease phenotype. When comparing the three disease progression time points in the SOD1-G37R mouse, both APLP2 and APP protein expression levels in the spinal cord were significantly higher at End-stage compared to both the pre-symptomatic and symptomatic stages ($p<0.01$, Figure 2A). In contrast, similar protein expression levels of APLP2 and APP were measured in the brainstem, cerebellum and hindlimb muscle and they were also similar when compared across the different disease progression time points in the SOD1-G37R mouse and again when compared to the age matched WT control group (Figure S1).

Female and male mice were compared to determine whether the elevated levels of APLP2 and APP protein expression levels in the spinal cord of the SOD1-G37R mouse at End-stage was sex dependent. While the APLP2 protein level was similarly upregulated in both sexes in the SOD1-G37R mouse at End-stage compared to the WT group, a statistical significance was only achieved for the male mouse ($p<0.05$, Figure 2B). The APP protein level was significantly upregulated in both sexes too in the SOD1-G37R mouse compared to respective WT littermate controls and it was also significantly higher in the male compared to the female SOD1-G37R mouse ($p<0.05$, Figure 2B). These results demonstrate that APP and APLP2 protein expression levels are significantly upregulated in the spinal cord at End-stage in SOD1-G37R mouse, an effect that is sex-dependent.

The lifespan is increased in female but not male SOD1-G37R mouse lacking APLP2 gene expression.

To determine whether modulating the APLP2 expression would affect the limiting 28 week lifespan of the SOD1-G37R mouse, the APLP2-/- mouse was crossbred with the SOD1-G37R mouse to generate three distinct mouse lines (SOD1-G37R:APLP2+/+, SOD1-G37R:APLP2+/- and SOD1-G37R:APLP2-/-) and their survival life expectancy was monitored for each sex (Figure 3). The most dramatic effect of APLP2 gene deletion was observed in the female SOD1-G37R:APLP2-/- mouse whereby its lifespan was significantly increased by two to three weeks compared to the SOD1-G37R:APLP2+/+ and SOD1-G37R:APLP2+/- (p=

0.0005 and p= 0.003 respectively, Figure 3B). In contrast, life expectancy was unchanged when comparing across the male mouse groups (Figure 3C). Next, we compared the male to female survival plots between the three different mouse lines and while there was no sex-dependent difference in the lifespan between male and female for the SOD1-G37R:APLP2+/+ mouse line (Figure 3D), the partial deletion of APLP2 gene in the SOD1-G37R:APLP2+/- mouse caused a longer lifespan in the male compared to the female mouse, an effect that was more pronounced in weeks prior to the End-stage of disease progression (p=0.0354, Figure 3E). In contrast, the mice with homozygous deletion of APLP2 (SOD1-G37R/APLP2-/-) resulted in a significantly extended lifespan by ~1.5 weeks in female compared to male mice (p=0.0058, Figure 3F). Collectively, these results demonstrate how the SOD1-G37R mouse lifespan and associated End-stage progression of this disease, is directly modulated by the extent of APLP2 gene expression and the sex of the mouse.

Motor performance is dysfunctional in female but not male SOD1-G37R mouse lacking APLP2 gene expression

It is well established that motor performance gradually deteriorates over time in the SOD1-G37R mouse as the disease phenotype progresses over time (42). Therefore, having established how APLP2 gene deletion significantly prolongs the lifespan of the female SOD1-G37R:APLP2-/- mouse, we next examined whether modulation of APLP2 gene expression affected their motor performance by testing them on an accelerating rotarod instrument (42). While the female SOD1-G37R:APLP2-/- and SOD1-G37R:APLP2+/- mice performed generally worse off on the rotarod test compared to the SOD1-G37R:APLP2+/+ mouse during the period of 8 to 25 weeks of age and a statistical difference was found only at 22 and 24 weeks of age ($p<0.01$, Figure 4A). In contrast, APLP2 gene deletion in the male SOD1-G37R mouse did not affect their motor performance based on their rotarod testing results (Figure 4B). When comparing female to male across the three genotype lines, the SOD1-G37R:APLP2+/+ female mouse displayed a general deficit and delay in motor performance compared to males from 21 weeks to End-stage of disease but this was significantly different only at the 22, 24 and 25 week time points ($p<0.05$, Figure 4C-4E).

To calculate the age of decline in motor performance between the three genotype lines, we opted for a more sophisticated analysis using the GenStat Statistical analysis software package. A split line regression model was used to divide the data into two regression lines to represent two different phases of motor performance. The first phase represents when the mouse performed at equilibrium or there was an incline in the motor performance test and the second phase is depicted when the animal showed a decline in their performance. The model then detects the precise regression breaks between the two regression lines and estimates the age of decline in the motor performance for each animal. Using this analysis strategy, the motor performance in the female mouse was significantly delayed compared to the male mouse in all three genotype lines ranging from ~3 weeks in both the SOD1-G37R:APLP2 +/+ and SOD1-G37R:APLP2+/- ($p<0.05$) and by ~ 6 weeks ($p<0.0001$) in the SOD1-G37R:APLP2-/- groups (Figure 4F). Given that no differences in the survival and motor performance were observed in the SOD1-

G37R:APLP2 groups, all male comparison data for the subsequent behavioural tests will not be discussed and data are provided in the supplementary information.

Neurological function score is improved in the female SOD1-G37R mouse lacking APLP2 gene expression

The effect of APLP2 deficiency on disease severity was examined by calculating the neurological function score based on the ALS TDI criteria (44, 49). Mice at the early disease stage (~8 weeks) were suspended by their tails and their left and right hindlimb extensions were monitored and scored up until End-stage disease. As expected, as disease symptoms develop and progress in this MND mouse model, left and right hindlimb extensions were impaired in all three SOD1-G37R:APLP2 genotypes and this was indicated by the progressive increase in the neurological scores for both female and male groups (Figure 5A and S2). We next compared the neurological scores for age and observed decreases in the neurological scores in the female SOD1-G37R:APLP2-/- mouse between 17 and 20 weeks of age, and significant at 18 weeks of age when compared with both SOD1-G37R:APLP2+/+ and SOD1-G37R:APLP2+/- for both left and right hindlimbs (Figure 5A). In comparison, the male SOD1-G37R:APLP2-/- mouse exhibited significantly improved neurological scores ($p<0.05$) in the right hindlimb at 24 and 25 weeks of age (Figure S2).

Consistent with the rotarod test, a sex comparison of the SOD1G-37R:APLP2+/+ (Figure 5B) showed a significantly better neurological function score in females at 23 weeks for left hindlimb and at 22 weeks for right hindlimb. The delay in symptoms onset was more pronounced for female SOD1G-37R:APLP2-/-, which was extended by ~ 4 weeks to reach a neurological score of 1 ($p<0.01$, Figure 5C). No differences were observed for the heterozygous SOD1G-37R:APLP2+/- group when sexes were analyzed separately for either left or right hindlimbs (Figure 5D). In summary, APLP2 deletion in the SOD1G-37R mouse is associated with altered neurological function since symptom onset is delayed and disease progression is altered, effects that were more pronounced in female mice.

Motor performance is improved prior to disease symptom onset in the female but not male SOD1-G37R mouse lacking APLP2 gene expression

Disease progression in MND can be characterised by gait deficits. Therefore, we used the DigiGait platform to monitor the mice as it provides a very comprehensive analysis of 54 different gait parameters. While three different speeds (10cm/s, 15cm/s and 20cm/s) were initially tested, only the data collected from the 15cm/s speed are presented since this speed allowed the mice to perform successfully on the instrument from early onset and until the late phase of disease detection. However, as the SOD1-G37R:APLP2 mouse lines progressed through to disease end-stage (data not shown), they were less likely to successfully perform on the DigiGait platform especially the male SOD1-G37R:APLP2-/-

mouse which were unable to complete the assessment task beyond 23 weeks of age. Of the 54 parameters that were assessed by DigiGait, significant changes were identified in 35 parameters and at different ages throughout the disease assessment period. We observed similar gait and body movement patterns between the different male SOD1-G37R:APLP2 genotypes for all limbs (Figure S3). We also detected similar gait patterns for the left and right fore-limbs of the female mice cohort. However, a significant difference was observed in the left and right hindlimbs of the female groups for stride length, swing, brake and propel. Therefore, only the hindlimb data of the female groups are shown. The female SOD1-G37R:APLP2-/- mouse displayed a significant improvement in stride length for both the left and right hindlimbs beginning at 11 weeks of age, and it remained higher than their female SOD1-G37R:APLP2+/+ counterparts as the disease progressed (Figure 6). The female SOD1-G37R:APLP2+/- mouse also exhibited a significant improvement in stride length, however, this was only significant at the later 12 and 18 weeks of age. Significant improvement in swing, brake and propel indices were also calculated at 11 and 12 weeks for the SOD1-G37R:APLP2-/- and SOD1-G37R:APLP2+/- female mouse respectively. Overall, the results from DigiGait data are in agreement with the neurological scores, indicating a lack or reduction in APLP2 expression is associated with improved gait function in the female SOD1-G37R mouse but they do not align with the rotarod data which indicated that the APLP2 KO female mouse had a worse motor phenotype at the earlier ages.

Motor neuron survival, astrogliosis or microgliosis in the lumbar spinal cord were unchanged in the SOD1-G37R mouse lacking APLP2 expression

We next evaluated whether the delayed motor performance measured in the female SOD1-G37R:APLP2-/- mouse may be explained by motor neuron degeneration in the spinal cord. To address this, α-motor neurons, which are the most vulnerable motor neuron in MND were identified in spinal cord sections by Nissl staining and their size and quanta were determined (Figure 7A). Since the diameter size of the larger α-motor neurons in transgenic SOD1 mouse strains range from 18 to 37 μm (50), we classified neurons with a diameter size greater than 20 μm as α-motor neurons for quantitative analysis. As expected, the transgenic SOD1-G37R mouse contained 4- to 5-fold lower numbers of α-motor neurons and this was significantly different to their WT littermate controls (Figure 7B). APLP2 gene deletion caused a 30% reduction in α-motor neurons numbers in the male mouse and this was significantly different compared to both its WT litter mate control and to the female WT:APLP2-/- mouse, but this sex difference was not recapitulated in the SOD1-G37R mouse model (Figure 7B). Taken together, these results suggest that APLP2 deficiency in the SOD1-G37R mouse does not affect motor neuron viability in this MND model.

Astrogliosis is a well characterized pathological feature of MND and has been reported in human ALS patients and transgenic animal models of familial ALS (51, 52). Therefore, we examined if APLP2 expression modulated the activation state of astrocytes by quantitating the percentage area of stained GFAP immunoreactivity in the spinal cord tissue sections across the different mouse lines. While the

percentage change in the GFAP stained area was significantly higher in both the female and male groups for SOD1-G37R:APLP2+/+, SOD1-G37R:APLP2-/- and SOD1-G37R:APLP2+/- mice when compared with their respective WT:APLP2 littermate controls, a sex-dependent comparison of GFAP expression in the different genotypes revealed a significant reduction in the female compared to male groups of both SOD1-G37R:APLP2+/+ and SOD1-G37R:APLP2+/- but not SOD1-G37R:APLP2-/- (Figure 7C).

Microglial activation, which parallels MND progression (51), was examined in the ventral horn of the spinal cord tissue sections by immunohistochemistry analysis. Therefore, microglial activation, which was assessed by calculating the percentage area change of Iba1 immunoreactivity, was significantly increased in the SOD1-G37R:APLP2 female and male cohorts compared to the WT littermate controls (Figure 7D). The only sex differences observed were in the WT:APLP2-/- mouse where by the females displayed significantly higher levels of microglial activation compared to male mice (Figure 7D).

APP protein level is reduced in the SOD1-G37R mouse lacking APLP2 expression

APP protein has been shown to have several important physiological roles (53, 54) and its expression is altered in different pathological diseases including MND (22) suggesting that it may have important roles in modulating disease progression. Since APLP2 and APP belong to the same gene family, we investigated if APLP2 deficiency in the SOD1-G37R mouse affected the APP protein expression level or patterns in various organs affected by MND. Brain, spinal cord and hindlimb muscles were harvested at End-stage of disease from SOD1-G37R:APLP2 and age matched WT:APLP2 littermates and endogenous APP protein expression quantitated by Western blotting analysis. APP protein expression level in whole brain lysate samples was similar across all mouse genotypes and between female and male cohorts too (Figure 8A).

In contrast, the spinal cord lysates contained significantly higher APP protein expression levels (~2-3 fold) in all SOD1-G37R:APLP2 genotypes for both female and male groups compared to the WT genotypes respectively (Figure 8B). To support this western blot data analysis, immunohistochemistry was performed and the intensity of APP immunoreactivity was detected in the ventral horn region of the lumbar spinal cord sections was quantitated and expressed relative to the WT control group (Figure S4C and S4D). In agreement with the western blot analysis, we observed a significant increase in total APP immunoreactivity relative to the WT control groups, in both sexes of the SOD1-G37R:APLP2+/+ mouse (Figure S4D). While the level of APP immunoreactivity remained significantly elevated in the male SOD1-G37R:APLP2+/- and SOD1-G37R:APLP2-/- mouse compared to the WT control group, the APP levels were partially decreased and significantly different to the SOD1-G37R:APLP2+/+ group (Figure S4D). In contrast to the male mice, the female mice displayed and unexpected finding where by mice lacking one or both APLP2 alleles displayed lower levels of APP immunoreactivity compared to both the female SOD1-G37R:APLP2+/+ mouse and male SOD1-G37R:APLP2-/- and SOD1-G37R:APLP2+/- respectively and levels were not different to WT groups too (Figure S4D). These contrasting results may be explained

by the differences in sample preparation since the whole spinal cord from the lumbar region was used for western blotting and only the small localized ventral horn region, which accounts for ~20% of the total surface area within the spinal cord tissue, was only assessed for immunohistochemistry analysis suggesting that focal APP expression levels differs within localized regions of the spinal cord in these MND mouse tissue.

In contrast to the neural tissue where an 87 kDa band was the major APP species present, the tissue lysates prepared from hindlimb muscle contained 2 prominent APP species with molecular weights of 87 and 55 and a third band that was both fainter and smaller at 25 kDa band (Figure 8C). The band intensity of the largest 87 kDa APP species was significantly higher in the female SOD1-G37R:APLP2-/- (~5.3 fold) and male SOD1-G37R:APLP2+/+ (~4.8 fold) mice when compared to WT:APLP2+/+ mice (Figure 8C). Further quantitative analysis of the smaller 55kDa and 25kDa APP immunoreactive bands were found to be not statistically different (Figure S4A and S4B).

APLP2 gene deletion exacerbates NMJ denervation in male SOD1 mice and improves NMJ innervation in the female SOD1-G37R mouse

Both APP and APLP2 are physiologically expressed in motor neurons and muscle tissue and especially in the NMJ where they provide important roles in its formation and maturation (30, 55-57). As expected, NMJ in the extensor digitorum longus of SOD1-G93A mouse, an alternative MND mouse model, displayed significant denervation while ablation of the APP gene in this mouse model reversed this phenotype and a significant decrease in the proportion of denervated NMJs was observed (22). In our studies, we examined the GA muscle at end-stage of disease and the NMJ was identified by indirect immunofluorescence and quantitating the extent of colocalization between alpha-bungarotoxin and synaptophysin (Figure 9A). Based on their innervation of the motor end plate, NMJs were classified into three groups, fully innervated (>20% colocalisation), partially innervated (10-20% colocalisation) or denervated (<10% colocalisation), where denervation of NMJs is revealed by a reduction in the number of ‘pretzel-shaped’ NMJs and these are accompanied by the collapse and fragmentation of NMJ structures (Figure 9A). Our results revealed that the female SOD1-G37R:APLP2-/- mice displayed a significantly higher proportion of fully innervated NMJs and a significantly decreased proportion of denervated NMJ when compared to both the SOD1-G37R:APLP2+/+ and SOD1-G37R:APLP2+/- mice groups (Figure 9B). In contrast, a mirror opposite effect was observed for the male SOD1-G37R:APLP2-/- mouse whereby these mice had significantly lower proportion of fully innervated NMJs and a significantly higher proportion of denervated NMJs compared to both SOD1-G37R:APLP2+/+ and SOD1-G37R:APLP2+/- mice groups (Figure 9C). Upon further analysis examining these sex based differences on the NMJ innervation pattern, we determined that there was a 3-fold significant lower proportion of the fully innervated NMJs with a concomitant 3-fold significant higher proportion of denervated NMJs in female compared to male SOD1-G37R:APLP2+/+ mice (Figure 9D). The SOD1-G37R:APLP2+/- mouse, which

partially expresses the APLP2 gene, the NMJ innervation pattern closely mirrored the significant changes observed when comparing the female and male SOD1-G37R:APLP2+/+ mice (Figure 9E). In contrast, a significantly higher proportion of fully innervated NMJs and a significantly lower proportion of denervated NMJs were calculated in the female SOD1-G37R:APLP2-/- mouse compared to its male group (Figure 9F). Taken together, our findings reveal a potential redundant role of APLP2 at the NMJ innervation and its component involvement may explain the delayed disease onset observed in the female SOD1-G37R:APLP2-/- mouse.

APLP2 gene deletion exacerbates muscle atrophy in male SOD1 mice but ameliorates atrophy in the female SOD1-G37R mouse

To investigate whether the deteriorating motor function in SOD1-G37R:APLP2 mice coincides with the progressive and widespread wasting observed in the hindlimb muscles, we performed transverse sections of the gastrocnemius muscle and the muscle myofibre types identified by ATPase staining and their cross-sectional area measured and binned into separate slow twitch Type 1 and fast twitch Type II fibre types according to their size (Figure 10). The muscle cell morphology in all different SOD1-G37R:APLP2 mouse lines at end-stage of disease progression were significantly compromised since the large muscle myofiber cell structures were dramatically smaller in appearance compared to the WT:APLP2+/+ and WT:APLP2-/- muscle tissue (Figure 10A). Quantification of the cross sectional area (CSA) of these myofiber cells between the SOD1-G37R:APLP2 mouse genotypes showed no change in the presence of the type I slow twitch muscle fibres and no difference was observed between female and male groups when comparing across the three SOD1-G37R:APLP2 genotypes examined (Figure 10B). In contrast, CSA type II muscle fibres, the most vulnerable type of muscle fibres in MND pathogenesis (58-60), were significantly reduced by ~40% in the male SOD1-G37R:APLP2-/- mouse compared to both SOD1-G37R:APLP2+/+ and SOD1-G37R:APLP2+/- mice groups (Figure 10C). The CSA Type II fibres was significantly increased in the female SOD1-G37R:APLP2-/- mouse compared to SOD1-G37R:APLP2+/+ (~24%) and SOD1-G37R:APLP2+/- mice (~53%, Figure 10C). While no changes were observed in the CSA of Type II fibres for male SOD1-G37R:APLP2+/- mice, a significant reduction in CSA was observed for female SOD1-G37R:APLP2+/- (~42%) when compared with SOD1-G37R:APLP2+/+ mice. Sex comparison of CSA across the different genotypes revealed a significant reduction in CSA in female groups of SOD1-G37R:APLP2+/+ and SOD1-G37R:APLP2+/- for Type II myofibres, but a significant reduction was observed in the male groups of SOD1-G37R:APLP2-/- mice (Figure 10C). These results parallel the NMJ results and highlight the potential involvement of skeletal muscle deficits of APLP2 deficiency affecting lower motor neuron pathology in SOD1 mice.

Discussion

The triggering event that causes MND is still largely unknown and hotly debated but there is good evidence that APP gene family play some important role in the pathology of this disease (27, 61, 62). This notion is strongly supported by our new findings showing APP and APLP2 protein expression are significantly elevated in spinal cord tissue isolated from post-mortem human MND cases compared to normal age matched control subjects. To further explore the role of these genes in MND, the SOD1-G37R mouse model was utilized since it replicates many of the human phenotypes including it causing these mice to die prematurely due to the significant damages associated with both the neuron and muscle cell physiology (42, 43, 63). We confirmed that both APP and APLP2 protein expression levels were also elevated in the spinal cord tissue lysates in the SOD1-G37R mouse model at the End-stage of this disease, a time where one would predict that the disease pathology would be very similar to the human stage of this disease. To further characterize the redundant roles of APP and more specifically APLP2 in this MND mouse model, we cross bred APLP2-/- mouse with the SOD1-G37R mouse, and this mating generated viable progeny containing the SOD1-G37R transgene that either lacked one or both APLP2 gene alleles. We found that in the SOD1-G37R mice lacking partial or total APLP2 expression exerted some beneficial effects especially on skeletal muscle function which was demonstrated by attenuated NMJ denervation, reduced muscle atrophy, ameliorated motor performance decline and together, this led to extended survival times that occurred in a sex-dependent manner.

The expression of APP protein was reported to be elevated in muscle of human patients with MND and in a the SOD1-G93A mouse model of MND (27) over time as the disease progressed, however, we did not see any detectable changes in either APP and APLP2 protein levels in skeletal muscle of the SOD1-G37R mouse model for MND throughout disease progression. This could be explained by the differences in MND mouse model examined since the pattern of SOD1 protein expression differs between tissue locations with higher concentrations typically detected in the spinal cord compared to hindlimb skeletal muscle (GA) (63, 64), or that the severity of this disease is associated with the level of tissue SOD1 protein expression (43). Since both APP and APLP2 expression is important in NMJ formation and maintenance during development (30, 56), their functional roles in MND may be associated with the phenomenon of NMJ degeneration being the triggering event in MND pathogenesis. The biochemical changes at the NMJs whereby significant improvement and reduction in denervation and muscle atrophy in the female SOD1-G37R:APLP2-/- mouse compared to SOD1-G37R:APLP2 wild-type littermates was observed suggests APLP2 may be directly involved with NMJ denervation in MND. While APP and APLP2 share functional similarities at the NMJ in MND pathogenesis, their expression may also have distinctly different effects in the CNS and PNS. These data, support the model that APLP2 may be associated with NMJ denervation in MND and that the distinct functional differences observed for APP and APLP2 suggests they may affect alternate signalling pathways in the pathophysiology of MND.

Apart from MND, the upregulation of APP has also been shown following TBI both in human and in animal models (65–67). In TBI cases, the upregulation of APP expression corresponds to a neuroprotective response in the localized area (23, 67). The potential of APP as a therapeutic agent was demonstrated by the intracerebroventricular administration of sAPPα in rats following TBI which successfully led to decreased axonal injury, reduced apoptosis and improved functional outcomes (68).

Moreover, when APP-KO mice were subjected to TBI, the lack of APP in this mouse made them more susceptible to injury resulting in poorer motor and cognitive outcomes, increased lesion volume and hippocampal damage compared to injured WT mice (69) while administration of sAPPα or APP96-110 in APP-KO mice prevented the TBI induced pathologies (70, 71). Therefore, the current TBI model proposes that the upregulation of APP protein expression in the nerve terminals following brain injury serves as an adaptive and neuroprotective response resulting from the injury (23, 70). This neuroprotective APP role does not apply to MND since genetic ablation of APP in the SOD1-G37R mouse was associated with decreased large motor neuron death and ameliorated NMJ denervation (22). Furthermore, increased APP expression was detected the spinal cord, the major disease site of MND, while brain content, the major site for TBI injuries, was unchanged highlighting the tissue site specificity of APP action. In our studies, the SOD1-G37R mouse contained elevated APP levels in the spinal cord only at the terminal disease End-stage period thus highlighting the narrow window in which elevated APP expression has the opportunity to exert its effects in the severely compromised tissue. These findings further illustrate the broad functional roles of APP protein in both health and especially disease environments with its many and distinct actions dependent on the type, duration, timing and especially the tissue site of disease or injury.

Through studies examining the APP family of knockout mice either independently or in combination, these have revealed non-redundant roles of APP and APLP2 demonstrating their critical expression in animal viability as well as providing us with a better understanding of their roles in normal physiology and in their involvement in disease development and progression. By assessing the redundant role of APLP2 in knockout mice, for example, these works identifies the important role of APLP2 and its association with a number of clinical diseases such as myopia (39), retinal synaptopathy, a congenital stationary night blindness condition (41) and in corneal epithelial wound healing (72). While exogenous treatment with recombinant APLP2 of chick sympathetic neurones promoted neurite outgrowth (31), endogenous elevated APLP2 levels have been associated with increased cellular growth of several cancer types, including pancreatic cancer (73, 74), colon cancer (75), breast cancer (76) and Ewing's sarcoma cell lines (77, 78) Therefore, to directly tested the role of APLP2 in MND, the SOD1-G37R mouse was by crossbred with the APLP2-/- mouse to generate viable progeny expressing SOD1-G37R:APLP2-/- and SOD1-G37R:APLP2+/- mouse lines which lacked both or one APLP2 allele respectively. A clear strength of our body of work is that both male and female sexes across the different animal lines were examined and this approach revealed how APLP2 gene ablation in the SOD1-G37R mouse resulted in a significant increase in survivability in the female but not male mice demonstrating a clear sex-based difference that would have been missed had we resorted to using single sex animal for our experiments. Our results contrast to the previous report examining the genetic ablation of APP in SOD1-G93A mice, in which only female mice were examined and although no significant extension in survivability was found in these cross bred mice, they did display a significant delay in disease onset or progression (22).

In the current study, the APLP2 levels in spinal cord of the SOD1-G37R mouse at disease End-Stage of disease were significantly higher in males compared to females and the different female SOD1-G37R:APLP2 genotypes displayed a slight delay in disease onset while the specific female SOD1-G37R:APLP2-/- mouse displayed delayed motor dysfunction during disease progression as well as longer

survival compared to the male counterpart. These sex based differences are not surprising since we previously reported how the female APLP2-/- mouse had better motor functions compared to its male counterpart and to WT littermates during ageing (79). However, the major sex differences we observed were limited to the End-Stage of disease progression as little or no effects seen at the earlier Symptomatic and Presymptomatic stages of MND classification suggesting little involvement of APLP2 prior to severe disease onset thus future studies looking at these parameters at earlier disease timepoints should be considered when examining MND disease progression. These cumulative observations highlight how a lack of APLP2 expression in females is beneficial and this may be exerting a partial protective effect on the development of neurodegenerative disease changes that can occur in ageing or in response to an oxidative stress response. Together, the effects of APLP2 on the pathological process of MND highlights a clear sex-dependent role.

Sex differences in human disease manifestations, progression and prevalence have been well noted in numerous illnesses including autoimmune disease (80), cardiovascular disease (81), cancers (82) and neurological disorders (83). Earlier studies reporting sex differences in MND with a slightly higher prevalence in men compared to women (1.5:1, male to female ratio) (5, 10) were later found to be supported by a dose response meta-analysis which showed that this sex-ratio decreased slightly with respect to population aging (84). This increased incidence in the male population is in line with the majority of epidemiological studies showing male MND patients tend to show an earlier age of disease onset (84), an effect that is also recapitulated in selective transgenic mouse models of MND (85, 86). Nevertheless, further clinical studies are needed to clarify the specifics of these sex differences involving SOD1 in MND and how APP and APLP2 contributes to this.

To further elucidate sex differences in the disease phenotype of the SOD1-G37R mouse lacking APLP2, sequence analysis of transcription factors in the promoter region of the mouse and human APLP2 gene was performed using the online transcription factor prediction program PROMO. We found multiple occurrences of the consensus sequence for transcription factor binding sites for progesterone, estrogen and androgen on both the mouse and human APLP2 genes (Figure S5). This analysis is supported by the earlier report illustrating how the estrogen receptor alpha (ERα), a key target for estrogen and most active in females, played a key role in the regulation of the mitochondrial proteostasis response in the SOD1-G93A mouse model for MND, an effect that was also sex dependent (87). Other sex-dependent differences in MND have been linked to peroxisome proliferator-activated receptor coactivator 1-alpha (PGC-1α), a master regulator of mitochondrial metabolism (88, 89). PGC-1α is a coactivator of ERα and regulates or enhances the transcriptional activity and signaling of androgen and estrogen receptors (90, 91). Since ablating PGC-1α gene expression in the SOD1-G93A mouse model for MND causes sex dependent shortened survival time in male but not female (92), this supports the possibility that the sex differences we observed in the SOD1-G37R are mediated by these sex hormones through there interaction APLP2. Whether this is linked to mitochondrial metabolism and PGC-1α is an avenue worth exploring in the future. Our data provide a novel pathway linking APLP2 expression with sex-dependent effects in MND that may explain the sexual dimorphism seen in MND. While questions regarding the overlapping

but distinct, functional roles of APP and APLP2 in MND remain unanswered, it is clear that APP and APLP2 can modulate the pathophysiology of MND in a sex-dependent manner.

Conclusion

Our study indicates a role for APLP2 (and APP) in sex-dependent differences in MND. Whether this opens the prospect for a female specific intervention for MND by targeting APLP2 function and/or expression remains unclear. A better understanding of the sex specific functions of APLP2 (and APP) in MND identifies novel ways to modulate MND disease and this highlights the necessity to consider the role of sex differences in the development of MND therapies.

Abbreviations

Alzheimer's Disease (AD), Amyloid Precursor Protein (APP), Amyloid Precursor-Like Protein 1 (APLP1), Amyloid Precursor-Like Protein 2 (APLP2), amyotrophic lateral sclerosis (ALS), Central Nervous System (CNS), Motor Neurone Disease (MND), Peripheral Nervous System (PNS)

Declarations

Ethical Approval and Consent to participate: All applicable international, national, and institutional guidelines for the care and use of animals were followed.

Publication: We confirm this manuscript has not been published elsewhere and is not under consideration for publication by another journal. All authors have approved the manuscript and agree with submission to *Molecular Neurodegeneration.*

Availability of supporting data: All data sets generated and analysed to support the conclusion of this study is included in this published article and its additional files.

Competing interests: We have no conflict of interest to declare.

Funding: This study was supported by National Health and Medical Research Council of Australia to RC and MND Research Australia (Betty Laidlaw and Jenny Barr Smith Research Grants to PJC and CAM, and Beryl Bayley Fellowship to JBWH). PHT was a recipient of a Nancy Frances Curry PhD Scholarship.

Authors' contributions: PHT designed and performed the experiments, JBWH and CAM processed contributed to the processing the result, GDJ performed the analysis, PHT, PJC, RC, GDJ contributed to writing of the manuscript. All authors read and approved the final manuscript.

Acknowledgements: We thank the School of Biomedical Sciences animal facility staff for their valuable assistance with animal care and handling, and the support provided by School of Biomedical Sciences Histology Facility. We thank Prof Sangram Sisodia for initially providing the APLP2 knockout mice.

References

1. Dharmadasa T, Henderson RD, Talman PS, Macdonell RA, Mathers S, Schultz DW, et al. Motor neurone disease: progress and challenges. The Medical journal of Australia. 2017;206(8):357-62.
2. Hardiman O, Al-Chalabi A, Chio A, Corr EM, Logroscino G, Robberecht W, et al. Amyotrophic lateral sclerosis. Nature reviews Disease primers. 2017;3:17071.
3. Nguyen HP, Van Broeckhoven C, van der Zee J. ALS genes in the genomic era and their implications for FTD. Trends in Genetics. 2018;34(6):404-23.
4. Grad LI, Rouleau GA, Ravits J, Cashman NR. Clinical Spectrum of Amyotrophic Lateral Sclerosis (ALS). Cold Spring Harbor perspectives in medicine. 2017;7(8).
5. McCombe PA, Henderson RD. Effects of gender in amyotrophic lateral sclerosis. Gend Med. 2010;7(6):557-70.
6. Ingre C, Roos PM, Piehl F, Kamel F, Fang F. Risk factors for amyotrophic lateral sclerosis. Clin Epidemiol. 2015;7:181-93.
7. Manjaly ZR, Scott KM, Abhinav K, Wijesekera L, Ganesalingam J, Goldstein LH, et al. The sex ratio in amyotrophic lateral sclerosis: A population based study. Amyotroph Lateral Scler. 2010;11(5):439-42.
8. Li TM, Alberman E, Swash M. Comparison of sporadic and familial disease amongst 580 cases of motor neuron disease. J Neurol Neurosurg Psychiatry. 1988;51(6):778-84.
9. Aggarwal A, Shashiraj. Juvenile amyotrophic lateral sclerosis. Indian J Pediatr. 2006;73(3):225-6.
10. Zoccolella S, Beghi E, Palagano G, Fraddosio A, Guerra V, Samarelli V, et al. Analysis of survival and prognostic factors in amyotrophic lateral sclerosis: a population based study. J Neurol Neurosurg Psychiatry. 2008;79(1):33-7.
11. Blasco H, Guennoc AM, Veyrat-Durebex C, Gordon PH, Andres CR, Camu W, et al. Amyotrophic lateral sclerosis: a hormonal condition? Amyotroph Lateral Scler. 2012;13(6):585-8.
12. Galvin M, Gaffney R, Corr B, Mays I, Hardiman O. From first symptoms to diagnosis of amyotrophic lateral sclerosis: perspectives of an Irish informal caregiver cohort—a thematic analysis. BMJ open. 2017;7(3):e014985.
13. Chio A, Mora G, Calvo A, Mazzini L, Bottacchi E, Mutani R, et al. Epidemiology of ALS in Italy: a 10-year prospective population-based study. Neurology. 2009;72(8):725-31.
14. Deliz B, Ramos K, Perez CM. Characterization of Patients with Amyotrophic Lateral Sclerosis attending the Muscular Dystrophy Association-Supported Clinics in Puerto Rico. Puerto Rico health sciences journal. 2018;37(1):5-11.
15. Van Den Bosch L. Genetic rodent models of amyotrophic lateral sclerosis. J Biomed Biotechnol. 2011;2011:348765.
16. Alexander GM, Erwin KL, Byers N, Deitch JS, Augelli BJ, Blankenhorn EP, et al. Effect of transgene copy number on survival in the G93A SOD1 transgenic mouse model of ALS. Brain Res Mol Brain Res. 2004;130(1-2):7-15.

17. Choi CI, Lee YD, Gwag BJ, Cho SI, Kim SS, Suh-Kim H. Effects of estrogen on lifespan and motor functions in female hSOD1 G93A transgenic mice. Journal of the neurological sciences. 2008;268(1-2):40-7.
18. Miana-Mena FJ, Munoz MJ, Yague G, Mendez M, Moreno M, Ciriza J, et al. Optimal methods to characterize the G93A mouse model of ALS. Amyotrophic lateral sclerosis and other motor neuron disorders : official publication of the World Federation of Neurology, Research Group on Motor Neuron Diseases. 2005;6(1):55-62.
19. Gould TW, Buss RR, Vinsant S, Prevette D, Sun W, Knudson CM, et al. Complete dissociation of motor neuron death from motor dysfunction by Bax deletion in a mouse model of ALS. J Neurosci. 2006;26(34):8774-86.
20. Kieran D, Woods I, Villunger A, Strasser A, Prehn JHM. Deletion of the BH3-only protein puma protects motoneurons from ER stress-induced apoptosis and delays motoneuron loss in ALS mice. Proc Natl Acad Sci U S A. 2007;104(51):20606-11.
21. Steinacker P, Hawlik A, Lehnert S, Jahn O, Meier S, Gorz E, et al. Neuroprotective function of cellular prion protein in a mouse model of amyotrophic lateral sclerosis. Am J Pathol. 2010;176(3):1409-20.
22. Bryson JB, Hobbs C, Parsons MJ, Bosch KD, Pandraud A, Walsh FS, et al. Amyloid precursor protein (APP) contributes to pathology in the SOD1(G93A) mouse model of amyotrophic lateral sclerosis. Hum Mol Genet. 2012;21(17):3871-82.
23. Plummer S, Van den Heuvel C, Thornton E, Corrigan F, Cappai R. The Neuroprotective Properties of the Amyloid Precursor Protein Following Traumatic Brain Injury. Aging Dis. 2016;7(2):163-79.
24. Xie YY, Yao ZB, Wu WT. Survival of motor neurons and expression of beta-amyloid protein in the aged rat spinal cord. Neuroreport. 2000;11(4):697-700.
25. Itoh T, Satou T, Nishida S, Tsubaki M, Hashimoto S, Ito H. Expression of amyloid precursor protein after rat traumatic brain injury. Neurol Res. 2009;31(1):103-9.
26. Sasaki S, Iwata M. Immunoreactivity of beta-amyloid precursor protein in amyotrophic lateral sclerosis. Acta neuropathologica. 1999;97(5):463-8.
27. Koistinen H, Prinjha R, Soden P, Harper A, Banner SJ, Pradat PF, et al. Elevated levels of amyloid precursor protein in muscle of patients with amyotrophic lateral sclerosis and a mouse model of the disease. Muscle & nerve. 2006;34(4):444-50.
28. Rabinovich-Toidman P, Rabinovich-Nikitin I, Ezra A, Barbiro B, Fogel H, Slutsky I, et al. Mutant SOD1 Increases APP Expression and Phosphorylation in Cellular and Animal Models of ALS. PloS one. 2015;10(11):e0143420.
29. Steinacker P, Hendrich C, Sperfeld AD, Jesse S, Lehnert S, Pabst A, et al. Concentrations of beta-amyloid precursor protein processing products in cerebrospinal fluid of patients with amyotrophic lateral sclerosis and frontotemporal lobar degeneration. Journal of neural transmission (Vienna, Austria : 1996). 2009;116(9):1169-78.
30. Wang P, Yang G, Mosier DR, Chang P, Zaidi T, Gong YD, et al. Defective neuromuscular synapses in mice lacking amyloid precursor protein (APP) and APP-Like protein 2. J Neurosci. 2005;25(5):1219-

25.

31. Cappai R, Mok SS, Galatis D, Tucker DF, Henry A, Beyreuther K, et al. Recombinant human amyloid precursor-like protein 2 (APLP2) expressed in the yeast Pichia pastoris can stimulate neurite outgrowth. FEBS letters. 1999;442(1):95-8.
32. Truong PH, Ciccotosto GD, Merson TD, Spoerri L, Chuei MJ, Ayers M, et al. Amyloid precursor protein and amyloid precursor-like protein 2 have distinct roles in modulating myelination, demyelination, and remyelination of axons. Glia. 2019;67(3):525-38.
33. Herms J, Anliker B, Heber S, Ring S, Fuhrmann M, Kretzschmar H, et al. Cortical dysplasia resembling human type 2 lissencephaly in mice lacking all three APP family members. EMBO J. 2004;23(20):4106-15.
34. Bergmans BA, Shariati SA, Habets RL, Verstreken P, Schoonjans L, Muller U, et al. Neurons generated from APP/APLP1/APLP2 triple knockout embryonic stem cells behave normally in vitro and in vivo: lack of evidence for a cell autonomous role of the amyloid precursor protein in neuronal differentiation. Stem Cells. 2010;28(3):399-406.
35. Shariati SA, Lau P, Hassan BA, Muller U, Dotti CG, De Strooper B, et al. APLP2 regulates neuronal stem cell differentiation during cortical development. J Cell Sci. 2013;126(Pt 5):1268-77.
36. Needham BE, Wlodek ME, Ciccotosto GD, Fam BC, Masters CL, Proietto J, et al. Identification of the Alzheimer's disease amyloid precursor protein (APP) and its homologue APLP2 as essential modulators of glucose and insulin homeostasis and growth. The Journal of pathology. 2008;215(2):155-63.
37. Needham BE, Ciccotosto GD, Cappai R. Combined deletions of amyloid precursor protein and amyloid precursor-like protein 2 reveal different effects on mouse brain metal homeostasis. Metallomics. 2014;6(3):598-603.
38. White AR, Reyes R, Mercer JF, Camakaris J, Zheng H, Bush AI, et al. Copper levels are increased in the cerebral cortex and liver of APP and APLP2 knockout mice. Brain Res. 1999;842(2):439-44.
39. Tkatchenko AV, Tkatchenko TV, Guggenheim JA, Verhoeven VJ, Hysi PG, Wojciechowski R, et al. APLP2 Regulates Refractive Error and Myopia Development in Mice and Humans. PLoS genetics. 2015;11(8):e1005432.
40. Dinet V, An N, Ciccotosto GD, Bruban J, Maoui A, Bellingham SA, et al. APP involvement in retinogenesis of mice. Acta neuropathologica. 2011;121(3):351-63.
41. Dinet V, Ciccotosto GD, Delaunay K, Borras C, Ranchon-Cole I, Kostic C, et al. Amyloid Precursor-Like Protein 2 deletion-induced retinal synaptopathy related to congenital stationary night blindness: structural, functional and molecular characteristics. Molecular brain. 2016;9(1):64.
42. Hilton JB, Kysenius K, White AR, Crouch PJ. The accumulation of enzymatically inactive cuproenzymes is a CNS-specific phenomenon of the SOD1(G37R) mouse model of ALS and can be restored by overexpressing the human copper transporter hCTR1. Exp Neurol. 2018;307:118-28.
43. Wong PC, Pardo CA, Borchelt DR, Lee MK, Copeland NG, Jenkins NA, et al. An adverse property of a familial ALS-linked SOD1 mutation causes motor neuron disease characterized by vacuolar

degeneration of mitochondria. Neuron. 1995;14(6):1105-16.
44. Ludolph AC, Bendotti C, Blaugrund E, Chio A, Greensmith L, Loeffler JP, et al. Guidelines for preclinical animal research in ALS/MND: A consensus meeting. Amyotroph Lateral Scler. 2010;11(1-2):38-45.
45. Luu L, Ciccotosto GD, Vella LJ, Cheng L, Roisman LC, Multhaup G, et al. Amyloid Precursor Protein Dimerisation Reduces Neurite Outgrowth. Mol Neurobiol. 2019;56(1):13-28.
46. Wasco W, Gurubhagavatula S, Paradis MD, Romano DM, Sisodia SS, Hyman BT, et al. Isolation and characterization of APLP2 encoding a homologue of the Alzheimer's associated amyloid beta protein precursor. Nature genetics. 1993;5(1):95-100.
47. White AR, Zheng H, Galatis D, Maher F, Hesse L, Multhaup G, et al. Survival of cultured neurons from amyloid precursor protein knock-out mice against Alzheimer's amyloid-beta toxicity and oxidative stress. J Neurosci. 1998;18(16):6207-17.
48. Hämäläinen N, Pette D. The histochemical profiles of fast fiber types IIB, IID, and IIA in skeletal muscles of mouse, rat, and rabbit. Journal of Histochemistry & Cytochemistry. 1993;41(5):733-43.
49. Leitner M, Menzies S, Lutz C. Working with ALS mice: Guidelines for preclinical testing & colony management. The Jackson Laboratory. 2009.
50. Zhou C, Zhang C, Zhao R, Chi S, Ge P, Zhang C. Human marrow stromal cells reduce microglial activation to protect motor neurons in a transgenic mouse model of amyotrophic lateral sclerosis. Journal of neuroinflammation. 2013;10:52.
51. Hall ED, Oostveen JA, Gurney ME. Relationship of microglial and astrocytic activation to disease onset and progression in a transgenic model of familial ALS. Glia. 1998;23(3):249-56.
52. Kushner PD, Stephenson DT, Wright S. Reactive astrogliosis is widespread in the subcortical white matter of amyotrophic lateral sclerosis brain. Journal of neuropathology and experimental neurology. 1991;50(3):263-77.
53. Dawkins E, Small DH. Insights into the physiological function of the beta-amyloid precursor protein: beyond Alzheimer's disease. J Neurochem. 2014;129(5):756-69.
54. Müller UC, Deller T, Korte M. Not just amyloid: physiological functions of the amyloid precursor protein family. Nature Reviews Neuroscience. 2017;18(5):281.
55. Akaaboune M, Allinquant B, Farza H, Roy K, Magoul R, Fiszman M, et al. Developmental regulation of amyloid precursor protein at the neuromuscular junction in mouse skeletal muscle. Mol Cell Neurosci. 2000;15(4):355-67.
56. Klevanski M, Saar M, Baumkotter F, Weyer SW, Kins S, Muller UC. Differential role of APP and APLPs for neuromuscular synaptic morphology and function. Molecular and cellular neurosciences. 2014;61:201-10.
57. Yang G, Gong YD, Gong K, Jiang WL, Kwon E, Wang P, et al. Reduced synaptic vesicle density and active zone size in mice lacking amyloid precursor protein (APP) and APP-like protein 2. Neuroscience letters. 2005;384(1-2):66-71.

58. Frey D, Schneider C, Xu L, Borg J, Spooren W, Caroni P. Early and selective loss of neuromuscular synapse subtypes with low sprouting competence in motoneuron diseases. J Neurosci. 2000;20(7):2534-42.
59. Pun S, Santos AF, Saxena S, Xu L, Caroni P. Selective vulnerability and pruning of phasic motoneuron axons in motoneuron disease alleviated by CNTF. Nat Neurosci. 2006;9(3):408-19.
60. Vinsant S, Mansfield C, Jimenez-Moreno R, Del Gaizo Moore V, Yoshikawa M, Hampton TG, et al. Characterization of early pathogenesis in the SOD1(G93A) mouse model of ALS: part II, results and discussion. Brain and behavior. 2013;3(4):431-57.
61. Bryson JB, Hobbs C, Parsons MJ, Bosch KD, Pandraud A, Walsh FS, et al. Amyloid precursor protein (APP) contributes to pathology in the SOD1G93A mouse model of amyotrophic lateral sclerosis. Hum Mol Genet. 2012;21(17):3871-82.
62. Herman AM, Khandelwal PJ, Rebeck GW, Moussa CE. Wild type TDP-43 induces neuro-inflammation and alters APP metabolism in lentiviral gene transfer models. Exp Neurol. 2012;235(1):297-305.
63. Hilton JB, White AR, Crouch PJ. Endogenous Cu in the central nervous system fails to satiate the elevated requirement for Cu in a mutant SOD1 mouse model of ALS. Metallomics. 2016;8(9):1002-11.
64. Gajowiak A, Stys A, Starzynski RR, Bednarz A, Lenartowicz M, Staron R, et al. Mice Overexpressing Both Non-Mutated Human SOD1 and Mutated SOD1(G93A) Genes: A Competent Experimental Model for Studying Iron Metabolism in Amyotrophic Lateral Sclerosis. Front Mol Neurosci. 2015;8(82):82.
65. Gentleman SM, Nash MJ, Sweeting CJ, Graham DI, Roberts GW. Beta-amyloid precursor protein (beta APP) as a marker for axonal injury after head injury. Neuroscience letters. 1993;160(2):139-44.
66. Pierce JE, Trojanowski JQ, Graham DI, Smith DH, McIntosh TK. Immunohistochemical characterization of alterations in the distribution of amyloid precursor proteins and beta-amyloid peptide after experimental brain injury in the rat. J Neurosci. 1996;16(3):1083-90.
67. Van den Heuvel C, Blumbergs PC, Finnie JW, Manavis J, Jones NR, Reilly PL, et al. Upregulation of amyloid precursor protein messenger RNA in response to traumatic brain injury: an ovine head impact model. Exp Neurol. 1999;159(2):441-50.
68. Thornton E, Vink R, Blumbergs PC, Van Den Heuvel C. Soluble amyloid precursor protein alpha reduces neuronal injury and improves functional outcome following diffuse traumatic brain injury in rats. Brain Res. 2006;1094(1):38-46.
69. Corrigan F, Vink R, Blumbergs PC, Masters CL, Cappai R, van den Heuvel C. Characterisation of the effect of knockout of the amyloid precursor protein on outcome following mild traumatic brain injury. Brain Res. 2012;1451:87-99.
70. Corrigan F, Vink R, Blumbergs PC, Masters CL, Cappai R, van den Heuvel C. sAPPalpha rescues deficits in amyloid precursor protein knockout mice following focal traumatic brain injury. J Neurochem. 2012;122(1):208-20.
71. Corrigan F, Thornton E, Roisman LC, Leonard AV, Vink R, Blumbergs PC, et al. The neuroprotective activity of the amyloid precursor protein against traumatic brain injury is mediated via the heparin

binding site in residues 96-110. J Neurochem. 2014;128(1):196-204.

72. Guo J, Thinakaran G, Guo Y, Sisodia SS, Yu FX. A role for amyloid precursor-like protein 2 in corneal epithelial wound healing. Invest Ophthalmol Vis Sci. 1998;39(2):292-300.
73. Peters HL, Tuli A, Wang X, Liu C, Pan Z, Ouellette MM, et al. Relevance of amyloid precursor-like protein 2 C-terminal fragments in pancreatic cancer cells. International journal of oncology. 2012;41(4):1464-74.
74. Peters OM, Ghasemi M, Brown RH, Jr. Emerging mechanisms of molecular pathology in ALS. The Journal of clinical investigation. 2015;125(5):1767-79.
75. Moss AC, Doran PP, Macmathuna P. In Silico Promoter Analysis can Predict Genes of Functional Relevance in Cell Proliferation: Validation in a Colon Cancer Model. Translational oncogenomics. 2007;2:1-16.
76. Abba MC, Drake JA, Hawkins KA, Hu Y, Sun H, Notcovich C, et al. Transcriptomic changes in human breast cancer progression as determined by serial analysis of gene expression. Breast cancer research : BCR. 2004;6(5):R499-513.
77. Peters HL, Yan Y, Nordgren TM, Cutucache CE, Joshi SS, Solheim JC. Amyloid precursor-like protein 2 suppresses irradiation-induced apoptosis in Ewing sarcoma cells and is elevated in immune-evasive Ewing sarcoma cells. Cancer biology & therapy. 2013;14(8):752-60.
78. Peters HL, Yan Y, Solheim JC. APLP2 regulates the expression of MHC class I molecules on irradiated Ewing's sarcoma cells. Oncoimmunology. 2013;2(10):e26293.
79. Truong PH, Ciccotosto GD, Cappai R. Analysis of Motor Function in Amyloid Precursor-Like Protein 2 Knockout Mice: The Effects of Ageing and Sex. Neurochemical research. 2018.
80. Ngo ST, Steyn FJ, McCombe PA. Gender differences in autoimmune disease. Front Neuroendocrinol. 2014;35(3):347-69.
81. Regitz-Zagrosek V, Kararigas G. Mechanistic Pathways of Sex Differences in Cardiovascular Disease. Physiological reviews. 2017;97(1):1-37.
82. Kim HI, Lim H, Moon A. Sex Differences in Cancer: Epidemiology, Genetics and Therapy. Biomol Ther (Seoul). 2018;26(4):335-42.
83. Pinares-Garcia P, Stratikopoulos M, Zagato A, Loke H, Lee J. Sex: A Significant Risk Factor for Neurodevelopmental and Neurodegenerative Disorders. Brain Sci. 2018;8(8):154.
84. Fontana A, Marin B, Luna J, Beghi E, Logroscino G, Boumédiene F, et al. Time-trend evolution and determinants of sex ratio in Amyotrophic Lateral Sclerosis: a dose-response meta-analysis. J Neurol. 2021.
85. Heiman-Patterson TD, Deitch JS, Blankenhorn EP, Erwin KL, Perreault MJ, Alexander BK, et al. Background and gender effects on survival in the TgN(SOD1-G93A)1Gur mouse model of ALS. Journal of the neurological sciences. 2005;236(1-2):1-7.
86. Heiman-Patterson TD, Sher RB, Blankenhorn EA, Alexander G, Deitch JS, Kunst CB, et al. Effect of genetic background on phenotype variability in transgenic mouse models of amyotrophic lateral

sclerosis: a window of opportunity in the search for genetic modifiers. Amyotroph Lateral Scler. 2011;12(2):79-86.

87. Riar AK, Burstein SR, Palomo GM, Arreguin A, Manfredi G, Germain D. Sex specific activation of the ERalpha axis of the mitochondrial UPR (UPRmt) in the G93A-SOD1 mouse model of familial ALS. Hum Mol Genet. 2017;26(7):1318-27.
88. Austin S, St-Pierre J. PGC1α and mitochondrial metabolism–emerging concepts and relevance in ageing and neurodegenerative disorders. J Cell Sci. 2012;125(21):4963-71.
89. Liang H, Ward WF. PGC-1alpha: a key regulator of energy metabolism. Advances in physiology education. 2006;30(4):145-51.
90. Shiota M, Yokomizo A, Tada Y, Inokuchi J, Tatsugami K, Kuroiwa K, et al. Peroxisome proliferator-activated receptor gamma coactivator-1alpha interacts with the androgen receptor (AR) and promotes prostate cancer cell growth by activating the AR. Mol Endocrinol. 2010;24(1):114-27.
91. Tcherepanova I, Puigserver P, Norris JD, Spiegelman BM, McDonnell DP. Modulation of estrogen receptor-alpha transcriptional activity by the coactivator PGC-1. J Biol Chem. 2000;275(21):16302-8.
92. Eschbach J, Schwalenstocker B, Soyal SM, Bayer H, Wiesner D, Akimoto C, et al. PGC-1alpha is a male-specific disease modifier of human and experimental amyotrophic lateral sclerosis. Hum Mol Genet. 2013;22(17):3477-84.

Figures

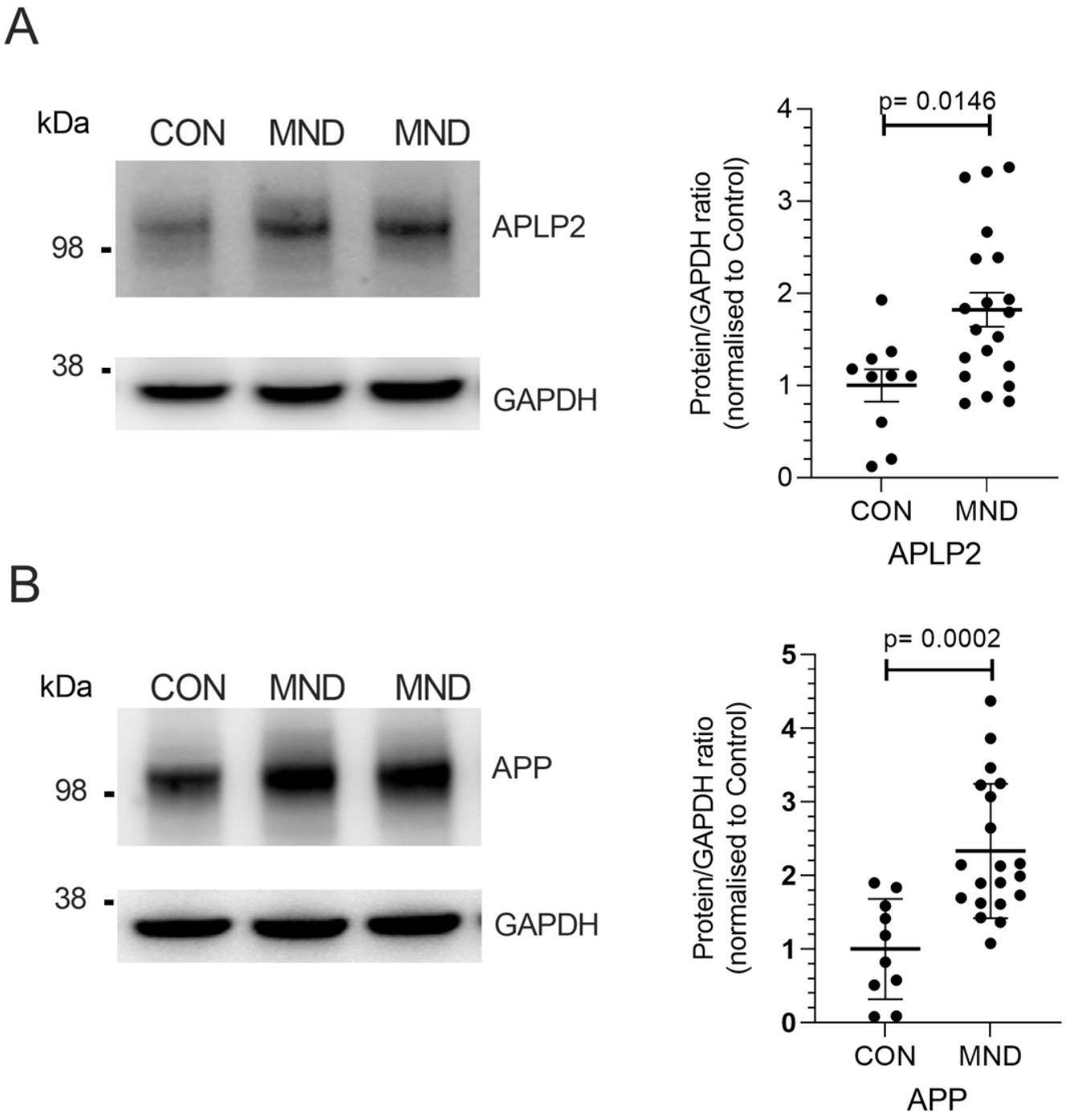

Figure 1

APP and APLP2 protein expression is increased in human, MND-affected spinal cord. Human spinal cord tissue samples were analysed by Western blot and densitometric quantification performed for (A) APLP2 and (B) APP protein. All APP and APLP2 data are normalised to the loading control GAPDH and protein expression level in MND samples expressed relative to Control cases. Data are shown as mean ± SEM, statistical significance was determined by Mann-Whitney unpaired t-test (n=10, 20).

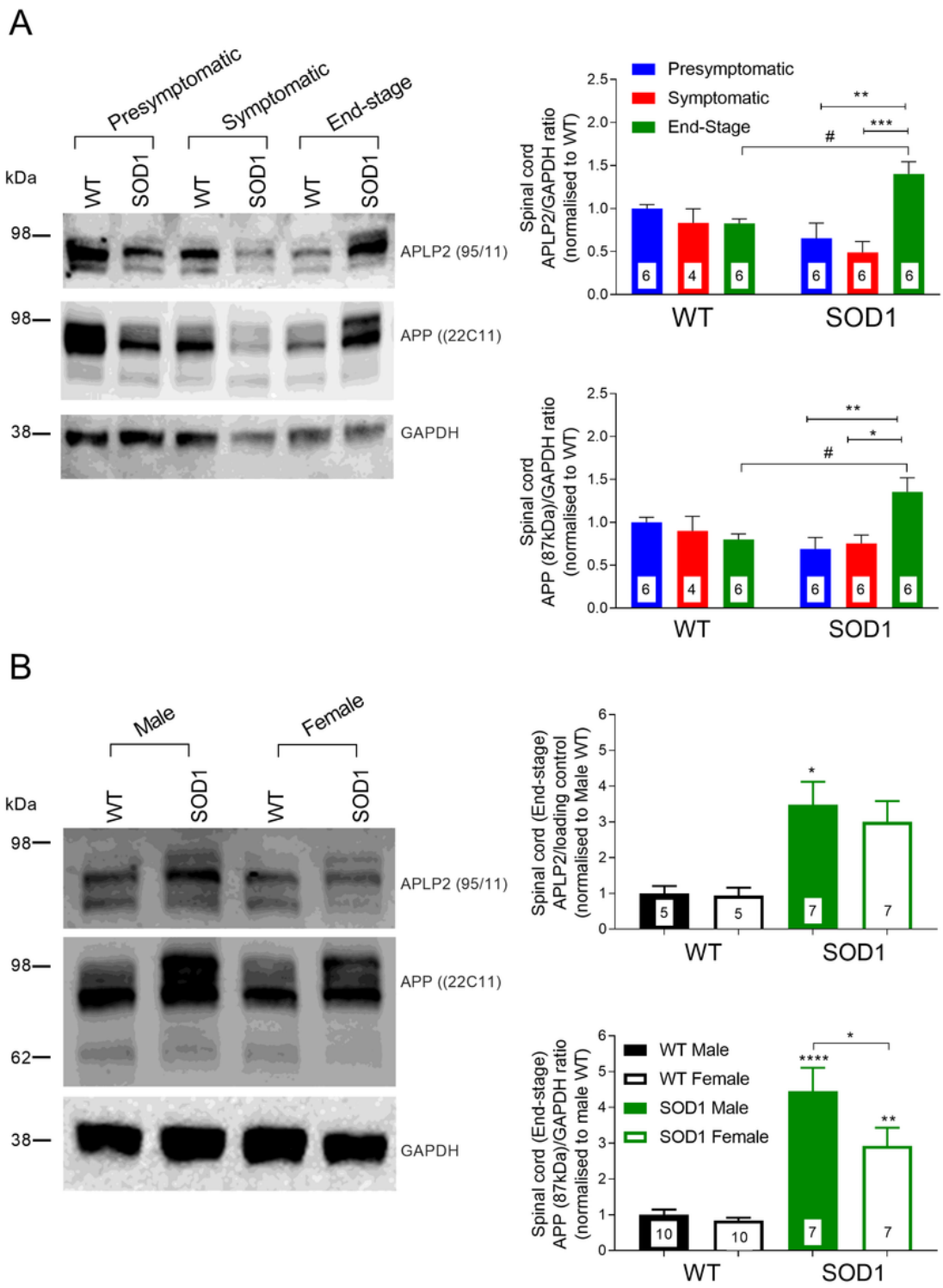

Figure 2

Elevation of APP and APLP2 levels in the spinal cord of SOD1-G37R during disease progression. Western blot images and densitometric quantification of spinal cord samples expressing APLP2 (antibody 95/11) and APP (antibody 22C11) protein in the (A) WT and SOD1-G37R mice (SOD1) at 12 weeks (pre-symptomatic, blue bar), 22 weeks (symptomatic, red bar) and 28 weeks (End-stage, green bar) and (B) male (filled bar) and female (open bar) of age-matched WT (black bar) controls and SOD1-G37R mouse

(green bar) at disease End-stage. Data were normalised to GAPDH loading control and expressed as a ratio of the WT pre-symptomatic sample for respective tissue samples. Data presented as mean ± SEM, *p<0.05, **p<0.01, ***p<0.001 compared between disease stage, #p<0.05 compared between WT and SOD1 using a two-way ANOVA with Bonferroni's post-hoc test. n=5-10.

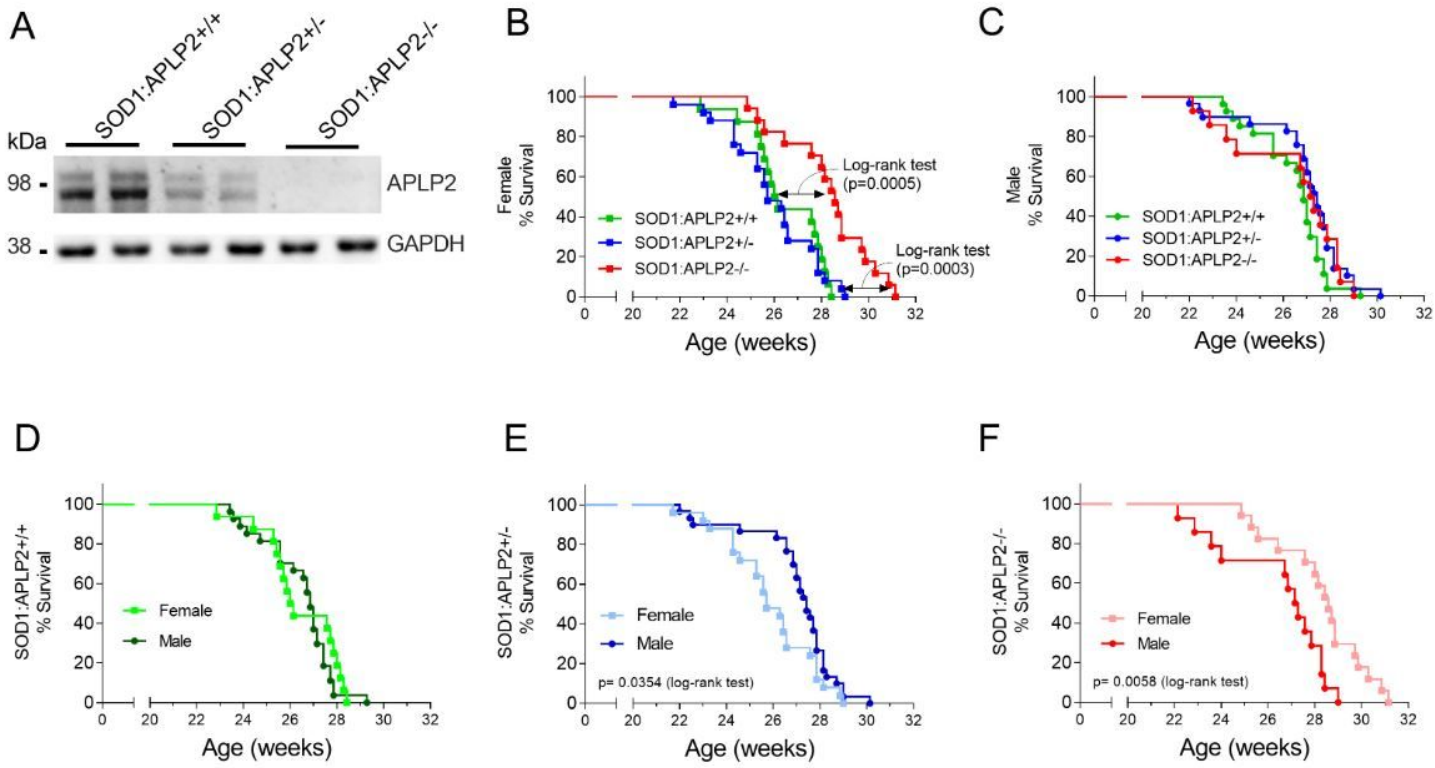

Figure 3

APLP2 deletion improves life span of female SOD1-G37R mice. (A) Western blot image of spinal cord tissue samples expressing APLP2 protein in crossbred mice for SOD1-G37R:APLP2+/+, SOD1-G37R:APLP2+/- and SOD1-G37R:APLP2-/- mice. Survival curves plotted for (B) female and (C) male for SOD1-G37R:APLP2+/+ (green), SOD1-G37R:APLP2+/- (blue) and SOD1-G37R:APLP2-/- (red) mice groups. Survival curves with log-rank (Mantel-Cox) test were compared between sexes for (D) SOD1-G37R:APLP2+/+, (E) SOD1-G37R:APLP2+/- and (F) SOD1-G37R:APLP2-/- mice. N=14-27.

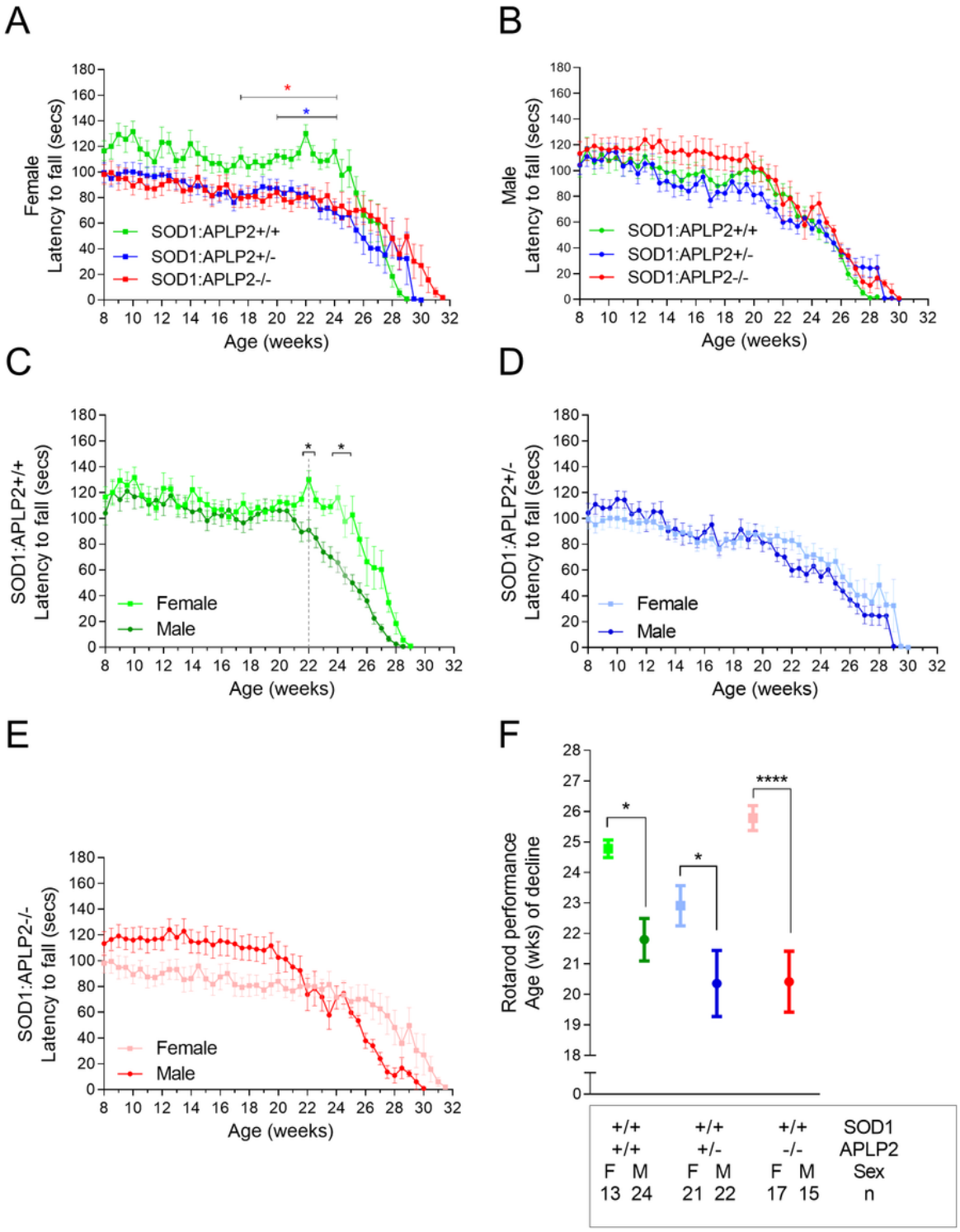

Figure 4

Motor performance dysfunction is delayed in female SOD1-G37R mice with APLP2 gene deletion. Motor performance function was assessed using the rotarod assay and data was recorded as latency to fall for (A) female and (B) male sexes of the SOD1-G37R:APLP2+/+ (green), SOD1-G37R:APLP2+/- (blue) and SOD1-G37R:APLP2-/- (red) mice genotypes. Direct male and female sex comparison was plotted and compared for (C) SOD1-G37R:APLP2+/+, (D) SOD1-G37R:APLP2+/- and (E) SOD1-G37R:APLP2-/- mice

cohorts. (F) The age of decline in weeks (wks) for rotarod performance was calculated using the split line regression model in GenStat analysis software. Data are shown as mean ± SEM, analysed using two-way ANOVA with Tukey's post-hoc test for comparison of rotarod performance across the weeks and by Student t-test for female (F) and male (M) sex comparison using the split line regression model, *p<0.05, **p<0.01, ****p<0.000, n=13-24 per group.

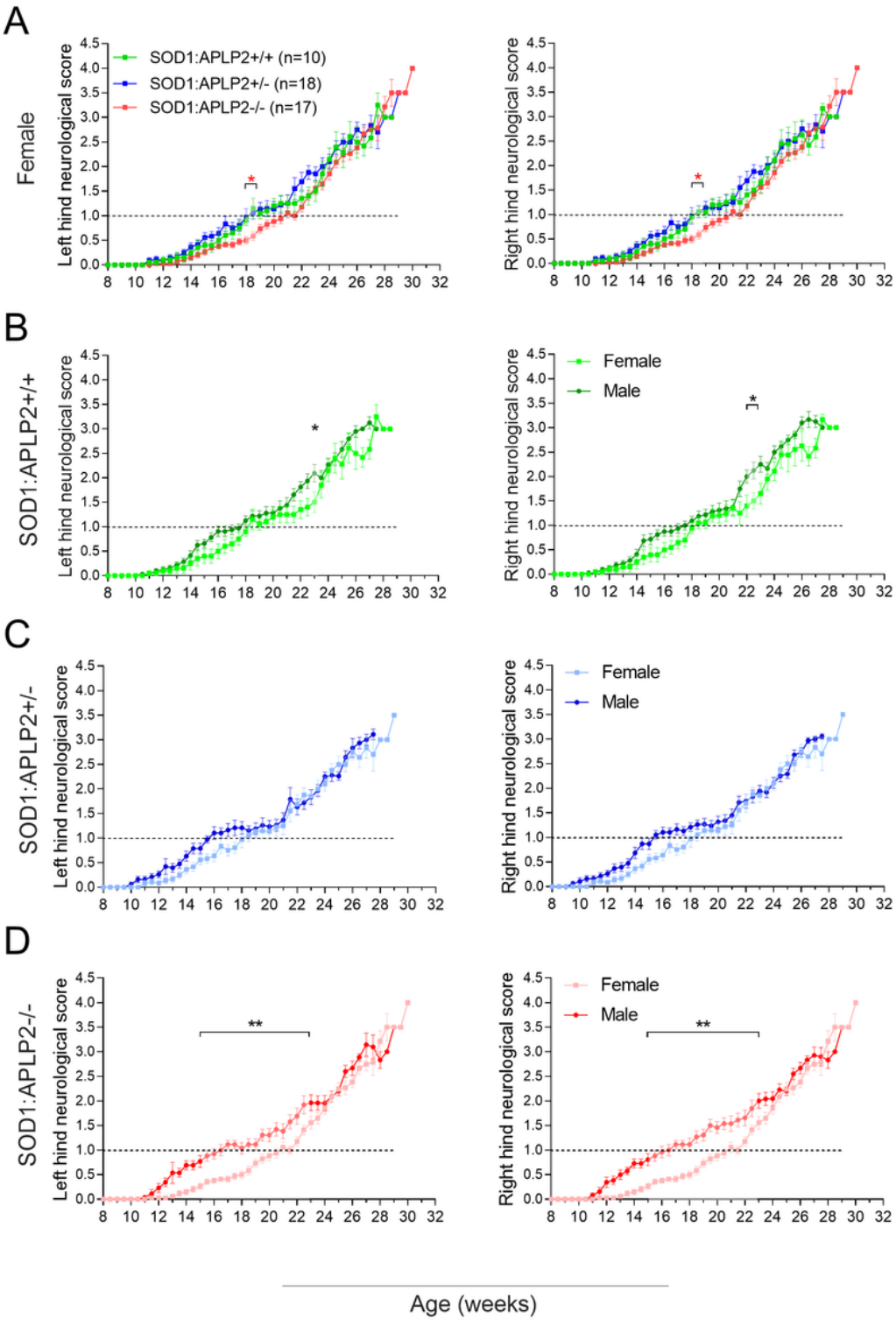

Figure 5

Female SOD1-G37R with APLP2 gene deletion showed delayed neurological function score compared to male mice. The effect of APLP2 gene deletion on the neurological function scores of SOD1-G37R mouse (SOD1) from 8 weeks of age until disease End-stage for the left and right hindlimbs was assessed for (A) female and (B) male groups of SOD1-G37R:APLP2+/+ (green), SOD1-G37R:APLP2+/- (blue) and SOD1-G37R:APLP2-/- (red) mice. Left and right hindlimb neurological function scores were compared between the female and male cohorts for (C) SOD1-G37R:APLP2+/+, (D) SOD1-G37R:APLP2+/- and (E) SOD1-G37R:APLP2-/-. Dashed horizontal lines indicate when mice reached a neurological function score of 1, an indication of when disease symptoms are prominent. Values presented as mean ± SEM. Statistical testing using two-way ANOVA with Tukey's post-hoc test, *$p<0.05$, **$p<0.01$. n=10-19.

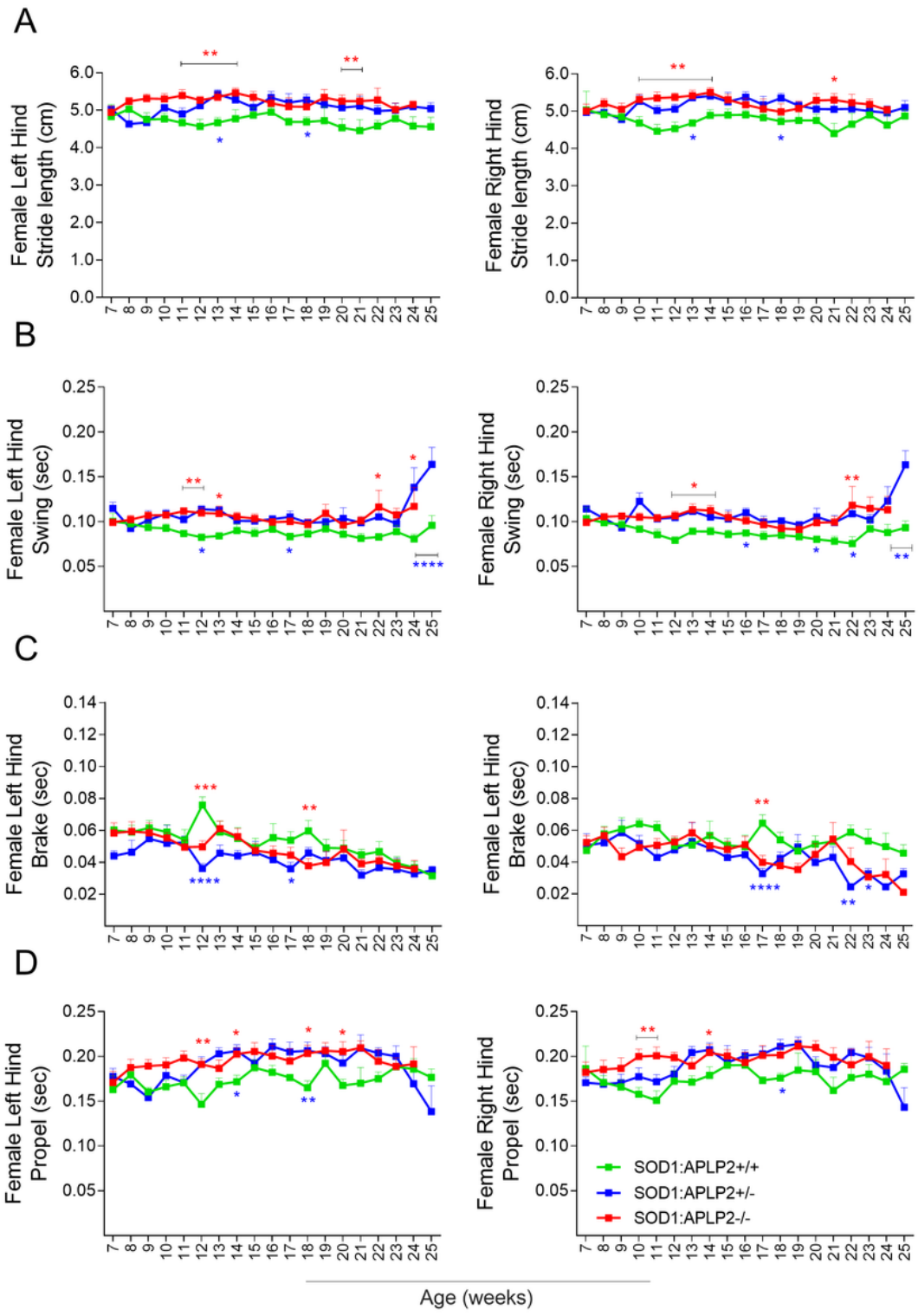

Figure 6

APLP2 deletion improves various hindlimbs gait indices of female SOD1-G37R mice prior to symptom onset. DigiGait analysis of left and right hindlimbs recorded at weekly intervals from 7-25 weeks of age and measurements for (A) stride length, (B) swing, (C) brake and (D) propel for female mice of SOD1;APLP2+/+ (green) , SOD1;APLP2+/- (blue) and SOD1;APLP2-/- (red) genotypes. Values presented

as mean ± SEM. Statistical testing comparing to SOD1-G37R:APLP2+/+ using two-way ANOVA with Tukey's post-hoc test, *p<0.05, **p<0.01, ****p<0.0001. n=5-8.

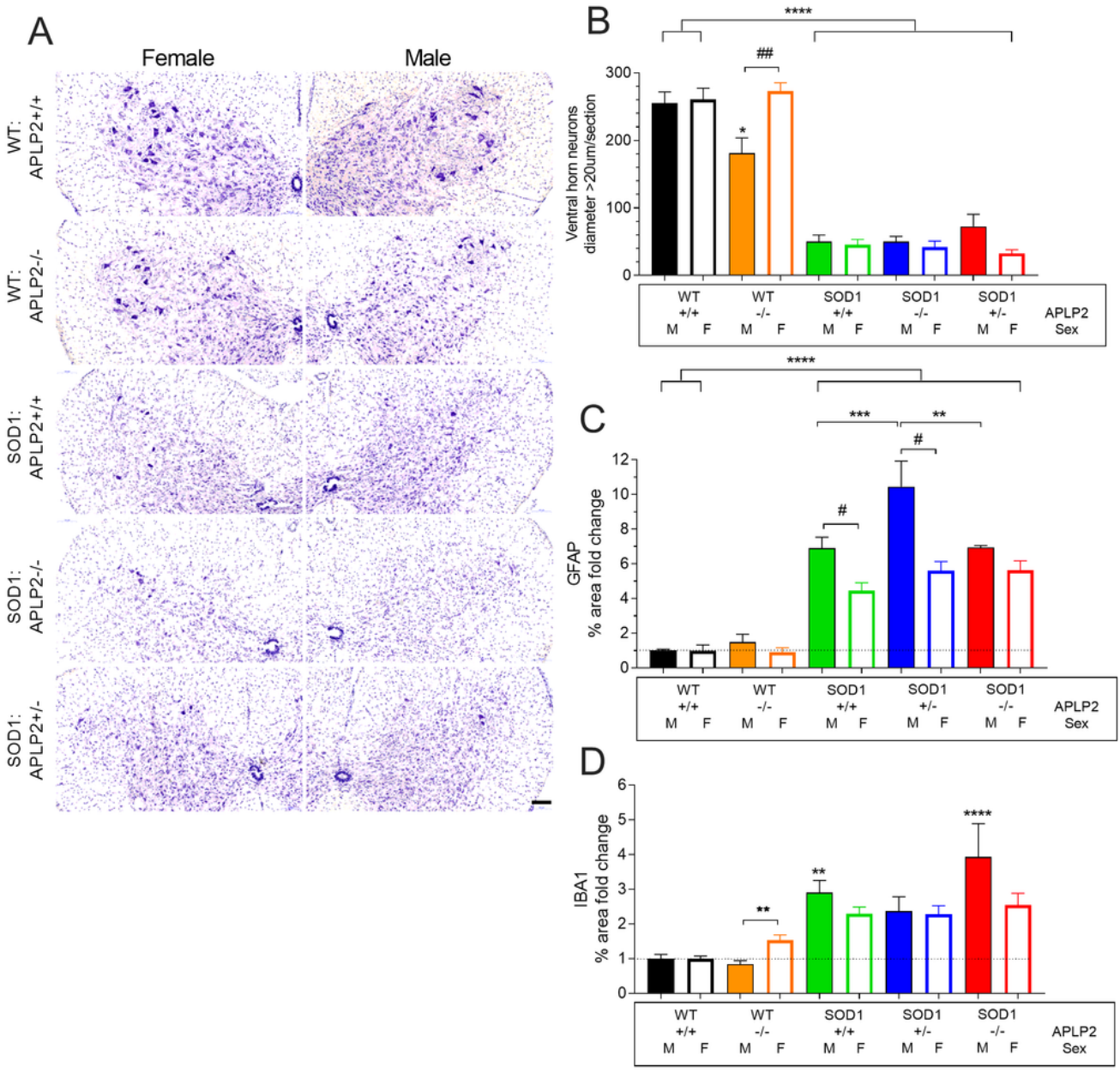

Figure 7

APLP2 gene deletion in SOD1-G37R mice does not affect motor neuron survival, astrogliosis and microgliosis. (A) Representative micrographs of motor neurons in the ventral horn of the spinal cord tissue sections stained with cresyl violet of female and male mice cohorts and at disease End stage for

SOD1-G37R (SOD1) and for WT:APLP2+/+, WT:APLP2-/-, SOD1-G37R:APLP2+/+, SOD1-G37R:APPLP2+/- and SOD1-G37R:APLP2-/- mice . Scale bar = 100μm. (B) Bar graphs representing the number of spinal neurons counted in 7 sections with a diameter >20 μm and located in the ventral horn region situated between L4 and L5 spinal cord segments for male (M) and female (F) mice. Quantitative analysis of the ventral horn lumbar spinal cord tissue sections immunolabelled with (C) anti-GFAP and (D) anti-IBA1 antibodies of WT:APLP2+/+, WT:APLP2-/-, SOD1-G37R:APLP2+/+, SOD1-G37R:APLP2+/- and SOD1-G37R:APLP2-/- mice at disease End-stage. Data shows the percentage fold change of areas positively immune-stained with GFAP and IBA-1 and then normalised to the respective female and male WT:APLP2+/+ mice groups. Values presented as mean ± SEM. Statistical testing by one-way ANOVA with Bonferroni's post-hoc test were used for genotype comparison to respective female and male WT:APLP2+/+ mice groups, *p<0.05, **p<0.01, ***p<0.001 and ****p<0.0001 and student t-test was used for comparison between sexes, #p<0.05, ##p<0.01. n=5-6.

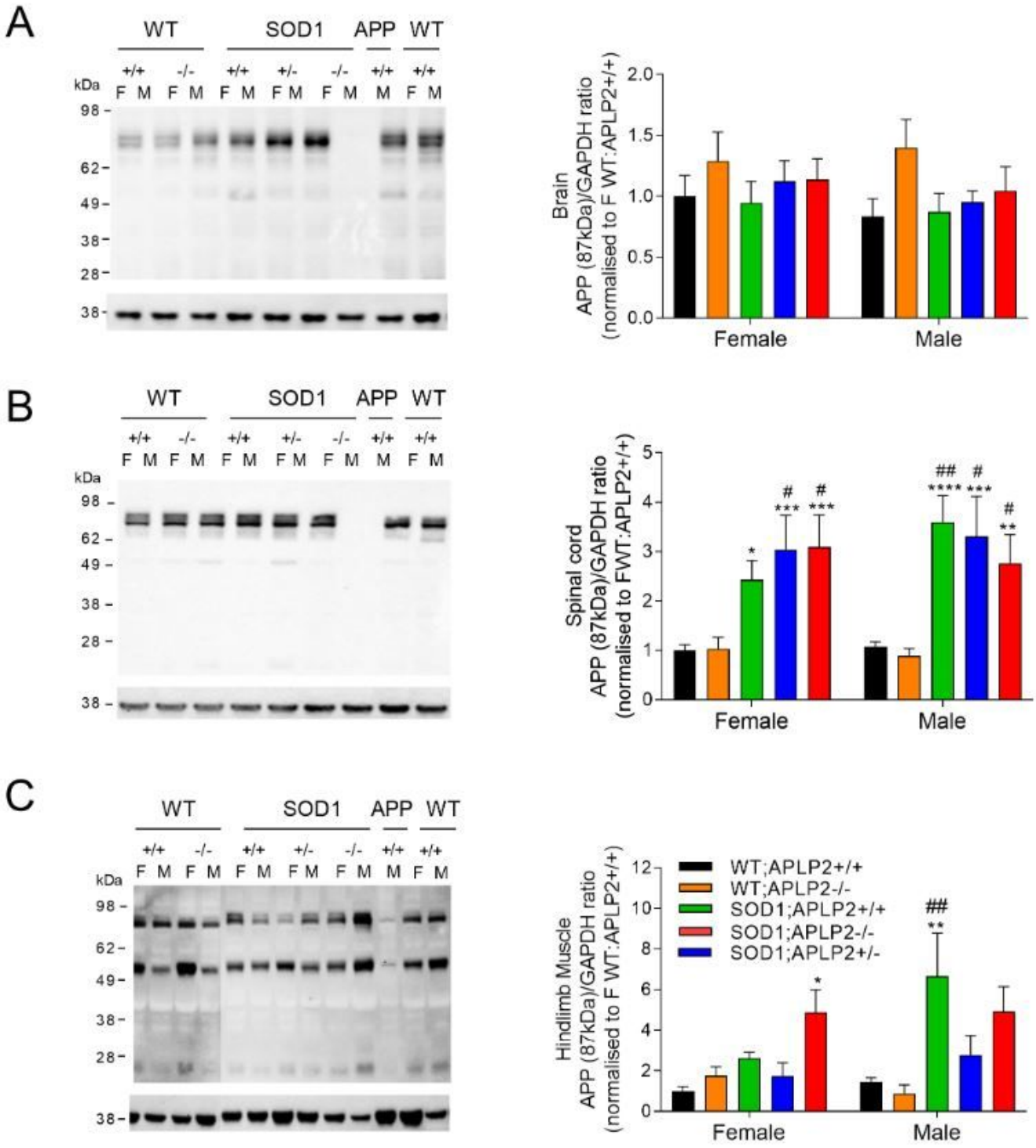

Figure 8

Genetic deletion of APLP2 gene decreases APP levels in the spinal cord of SOD1-G37R mice. Representative immunoblots and densitometric quantification of the full length ~87kDa APP band in the (A) brain (B) spinal cord and (C) hindlimb muscles of SOD1-G37R:APLP2+/+, SOD1-G37R:APLP2+/-, SOD1-G37R:APLP2-/- mice at disease end-stage and WT:APLP2+/+, WT:APLP2-/- age-matched littermate controls. For each respective tissues APP-/- and WT:APLP2+/+ mice were used as negative and positive

controls respectively. Values presented as mean ± SEM. Statistical testing by one-way ANOVA with Bonferroni's post-hoc test, *p<0.05, **p<0.01, ***p<0.001 and ****p<0.0001 compared to WT:APLP2+/+, #p<0.05 and ##p<0.01 compared to WT:APLP2-/- mice. n=4-6.

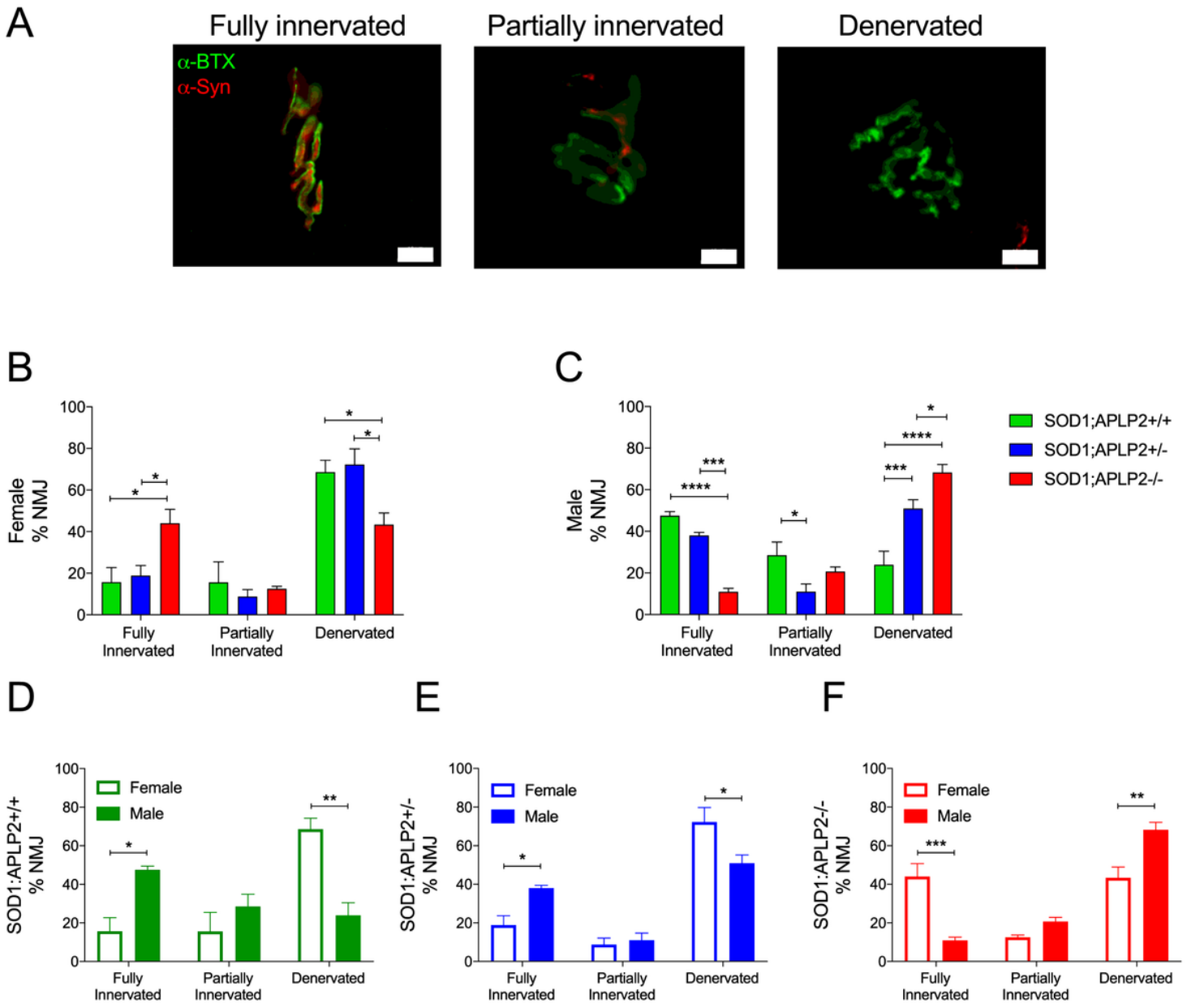

Figure 9

APLP2 gene deletion ameliorates NMJ denervation in female SOD1 mice. (A) Representative images of colocalization between pre-synaptic and post-synaptic marker defined as fully innervated, partially innerved and denervated NMJ. Scale bar=10μm. Arrows indicated collapsed and fragmented NMJ. Calculated percentages of fully innervated NMJ (>20% colocalisation), partially innervated NMJ (10-20% colocalisation) and denervated NMJ (<10% colocalisation) in three muscle sections (100μm apart) for (B) male and (C) female SOD1-G37R:APLP2+/+, SOD1-G37R:APLP2-/- and SOD1-G37R:APLP2+/- mice groups. NMJ innervation status was also compared between sexes for (D) SOD1-G37R:APLP2+/+, (E) SOD1-G37R:APLP2+/- and (F) SOD1-G37R:APLP2-/-. Data presented as mean ± SEM and statistical

testing by one-way ANOVA with Bonferroni's post-hoc test, *p<0.05, **p<0.01, ***p<0.001, ****p<0.0001, n=3-4.

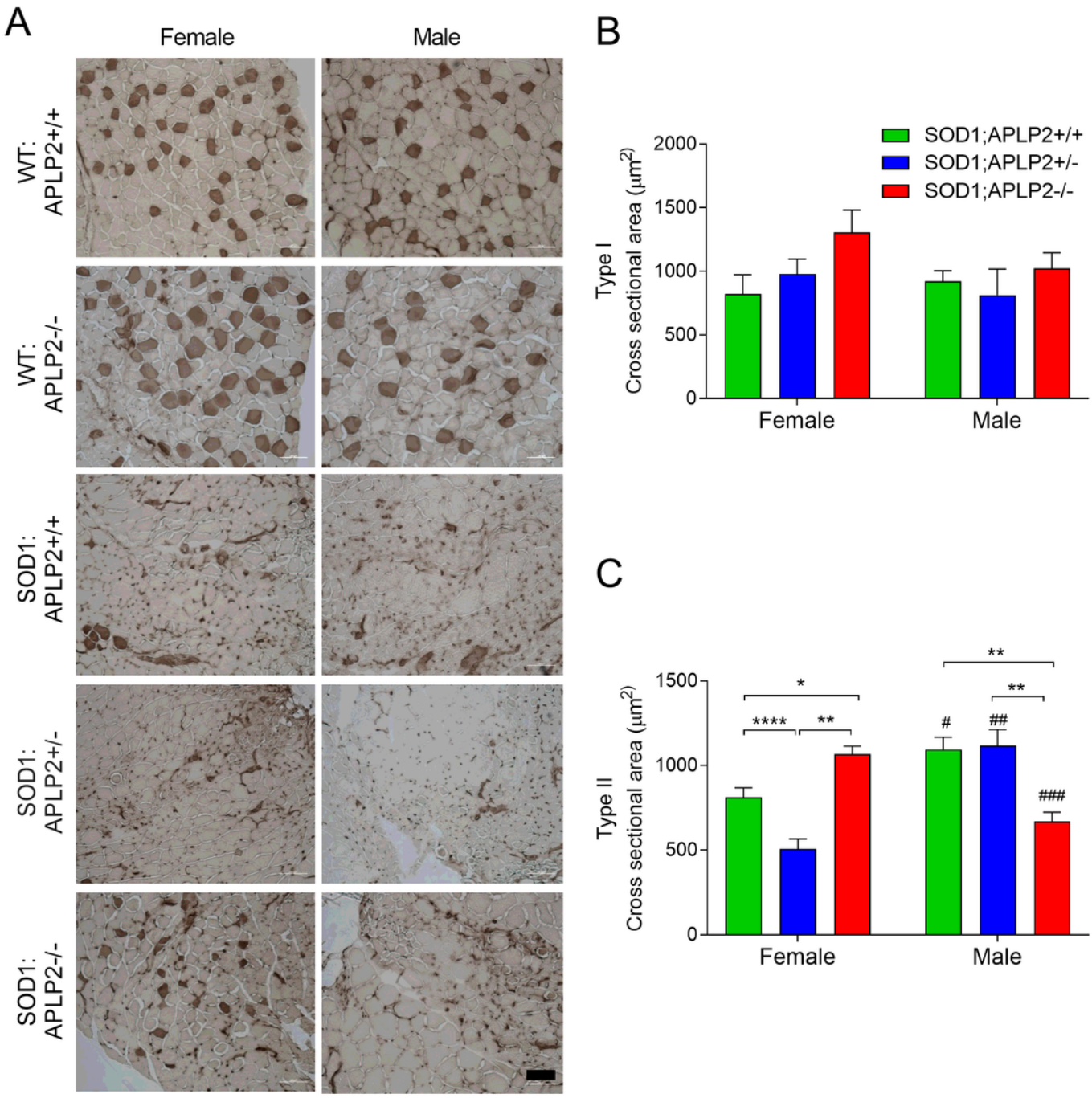

Figure 10

Genetic deletion of APLP2 expression in female mutant SOD1-G37R mice improves muscle fibre atrophy. (A) Representative micrographs of gastrocnemius muscle cross-sections stain with ATPase (pH 4.3) from female and male SOD1: APPLP2+/+, SOD1-G37R:APLP2+/-, SOD1-G37R:APLP2-/- at the end-stage of disease and their age-matched WT littermates control WT:APLP2+/+ and WT:APLP2-/-. Quantification of (B) slow twitch/type I and (C) fast twitch/type II myofibres cross-sectional area for both female and male groups of SOD1: APPLP2+/+, SOD1-G37R:APLP2+/-, SOD1-G37R:APLP2-/- at disease end-stage and (F-

H) sex comparison within the same genotype. Data present as mean ± SEM and statistical testing by one-way ANOVA with Bonferroni's post-hoc test were used for genotype comparison within the same sex, *p<0.05, **p<0.01, ***p<0.001, ****p<0.0001, and student t-test was used for sex comparison within the same genotype, #p<0.05, ##p<0.01, ###p<0.001. n=4-6. Scale bar = 100μm.

Supplementary Files

This is a list of supplementary files associated with this preprint. Click to download.

- SuppFig1.tif
- SuppFig2.tif
- SuppFig3.tif
- SuppFig4.tif
- SuppFig5.tif